International Journal of Applied Mathematics

Volume 38 No. 1 2025, 73–150
ISSN: 1311-1728 (printed version); ISSN: 1314-8060 (on-line version)
doi: http://dx.doi.org/10.12732/ijam.v38i1.5

REVISITING FINITE DIFFERENCE SOLUTIONS FOR HEAT-TYPE EQUATIONS. PART II. ADVECTIVE TRANSFER

G. Garrido [1,§] , J. L. G. Pestaña [2]

[1] Departamento de Informática

Universidad de Jaén

Campus Las Lagunillas, 23071 Jaén, SPAIN

e-mail: ggluque@ujaen.es (corresponding author)

[2] Departamento de Física

Universidad de Jaén

Campus Las Lagunillas, 23071 Jaén, SPAIN

e-mail: jlg@ujaen.es

Abstract

In this second paper of a series, we revisit all major systematic uncertainties that affect a complete and unbiased sample of eleven finite difference schemes for advection-like equations. In order to provide the coherent picture, unlike the existing way, we use as the key tenets both

Received: December 27, 2024

the reverse Taylor's analysis and the discrete Fourier's analysis, as well as the monotonicity analysis. For every type of scheme, their theoretical uncertainties are examined. A detailed graphical investigation is also provided and used to give a physical reinterpretation of the Courant-Friedrichs-Lewy condition. We find that no scheme considered in this study resolves the smaller length scales well. Furthermore, we present several numerical experiments on an equal footing corroborating our demonstrations and proving to what degree the accuracy of each scheme is impaired by the discontinuities in the data. A comparison with each other is made as well. We definitively establish that the ingenious Lax-Wendroff scheme is preferred by experiments.

Math. Subject Classification: 35K05, 35L02, 65M06, 65N22, 97N40

Key Words and Phrases: heat equation; first-order hyperbolic equations; finite difference methods for initial value and initial-boundary value problems involving PDEs; numerical solution of discretized equations for boundary value problems involving PDEs; numerical analysis (educational aspects)

1. Introduction

We plan to numerically integrate the advective-diffusive transfer process, which is yet to be fully understood [1]. In the first paper of this series [2, hereafter referred to as Part I] we re-investigated how well finite difference schemes solve the diffusive transfer and how we can qualitatively (based on the Hirt's formalism) and quantitatively (based on the von Neumann's formalism) describe their uncertainties, which allowed us to conclusively assess the importance of various approximations. Hence, we now wish an equally deep dive into advective transfer.

The scope of this Part II is exactly to integrate the simplest (Dirichlet, linear and unidimensional) hyperbolic differential equation using all at most three-level, low-order schemes. Also, we do it in the chronological sequence in which they were developed. While doing so, we explain all the methodological insights and concerns of the difference equation needed to follow the very recent review by Sagaut et al. [1]. This is the position of our entry-level paper with respect to the state of art. However, in what follows we will not review the principles of this finite difference approach but refer the reader to Part I for their details and clarification of notation.

The paper is organized as follows. In Section 2 we rigorously investigate all eleven pioneering schemes which our topical current understanding of hyperbolic differential equations is based on, namely the Richardson's, Schmidt's, Crank-Nicolson, Laasonen's, Courant-Isaacson-Rees, Lax's, Lax-Richtmyer, Wendroff's, Lax-Wendroff, Molenkamp's and Lerat's schemes. In Section 3 we implement all of these schemes. Then, as a proof of concept, we both discuss their performance properties and eventually compare them with each other. Finally Section 4 presents a short summary and conclusive remarks, highlighting the differences between the dissipative couplings of Part I and the dynamical couplings of Part II. Motivated in particular by discontinuities in the data, A shows the exemplary initial value problem, as simple as it is very interesting, we apply in Section 3.

2. **The difference equations**

In this section we lay groundwork for detailed follow-up performance tests. We thoroughly revisit the finite difference equations for canonical linear advection equation, Eq. (2.17) of Part I, up to second order in the derivatives and also carefully examine the sources and form of their theoretical uncertainties, i.e. we answer analytically to consistency, stability and convergence criteria. We highlight the conceptual differences between not only hierarchical and monolithic schemes but also notably two and three level hierarchical schemes. We also show for the first time the risk of spatial oscillations throughout the entire range of wavenumbers, that is to say we examine separately all the Fourier components of the spatial variation. We sort the exposition, motivated by technical considerations lacking in literature, by chronology and acknowledging their authors.

To aid comparison with our canonical linear advection equation we note that the exact growth factor is unity, the exact propagation velocity is the constant v and we shall represent exact phase angle, $-C\,k\Delta x$, in every scheme.

2.1. **The Richardson's 1910 three-time-level explicit scheme.**

2.1.1. **Construction.** In 1910 Richardson [6] devised the pioneering scheme which was explicit in time and gave values at any time level in terms of values at the previous two time levels. To achieved this, he discretized both time and space derivatives by second order central differences, Eqs.

(2.9) and (2.10) of Part I respectively, i.e.,

$$\frac{T_j^{n+1} - T_j^{n-1}}{2\Delta t} = -v\frac{T_{j+1}^n - T_{j-1}^n}{2\Delta x}. \tag{2.1}$$

However, as a three-time-level bottom-up scheme that it is, the Richardson's scheme has the problem of setting the initial grid function value; i.e. we have to decide how start the process. The solution is to use any other single-step scheme, as shortly discussed.

TABLE 1. Schemes analysed in this work. Note that n represents the temperature at the current time step whereas $n+1$ (colored in red) represents the new (future) temperature. Note also the temperature one time step in the past, $n-1$ (colored in violet).

Author	Algorithm
Richardson [6]	$T_j^{n+1} = T_j^{n-1} + C\,(T_{j-1}^n - T_{j+1}^n)$
Schmidt [8]	$T_j^{n+1} = T_j^n - 0.5\,C\,(T_{j+1}^n - T_{j-1}^n)$
Crank-Nicolson [9]	$-0.25\,C\,T_{j-1}^{n+1} + T_j^{n+1} + 0.25\,C\,T_{j+1}^{n+1} = 0.25\,C\,T_{j-1}^n + T_j^n - 0.25\,C\,T_{j+1}^n$
Laasonen [11]	$-0.5\,C\,T_{j-1}^{n+1} + T_j^{n+1} + 0.5\,C\,T_{j+1}^{n+1} = T_j^n$
Courant-Isaccson-Rees [12]	$T_j^{n+1} = (1-C)\,T_j^n + C\,T_{j-1}^n$
Lax [13]	$T_j^{n+1} = 0.5\,(1-C)\,T_{j+1}^n + 0.5\,(1+C)\,T_{j-1}^n$
Lax-Richtmyer [14]	$-0.5\,C\,T_{j-1}^{n+1} + T_j^{n+1} + 0.5\,C\,T_{j+1}^{n+1} = 0.5\,(T_{j-1}^n + T_{j+1}^n)$
Wendroff [15]	$(1-C)\,T_{j-1}^{n+1} + (1+C)\,T_j^{n+1} = (1+C)\,T_{j-1}^n + (1-C)\,T_j^n$
Lax-Wendroff [16]	$T_j^{n+1} = 0.5\,(C^2+C)\,T_{j-1}^n + (1-C^2)\,T_j^n + 0.5\,(C^2-C)\,T_{j+1}^n$
Molenkamp [17]	$-C\,T_{j-1}^{n+1} + (1+C)\,T_j^{n+1} = T_j^n$
Lerat [18]	$0.5\,(-C^2-C)\,T_{j-1}^{n+1} + (1+C^2)\,T_j^{n+1} + 0.5\,(-C^2+C)\,T_{j+1}^{n+1} = T_j^n$

For easy reference we reformulate Eq. (2.1) in the second column in Table 1 introducing, for convenience, the so-called dimensionless Courant-Isaacson-Rees number:

$$C = v\frac{\Delta t}{\Delta x}, \tag{2.2}$$

which, like the dimensionless Fourier number solutions of parabolic partial differential equations (e.g. see Part I), provides a measure for the spatiotemporal discretization.

2.1.2. **Consistency and order of accuracy.** We firstly analyze the consistency of the scheme using the Hirt's method. Substituting each value of the grid function at points other than point (x_j, t^n) in the scheme

in a Taylor series around the value T_j^n at that point (x_j, t^n), i.e. substituting Eqs. (2.6), (2.8), (2.12) and (2.13) of Part I in Eq. (2.1), gives

$$\frac{\partial T}{\partial t} + v\frac{\partial T}{\partial x} = -\frac{v\,(\Delta x)^2}{6}\frac{\partial^3 T}{\partial x^3} - \frac{(\Delta t)^2}{6}\frac{\partial^3 T}{\partial t^3} + \cdots . \tag{2.3}$$

We then see from that equation, which is not yet the modified equation, that its right hand side vanishes when $\Delta t \to 0$ and $\Delta x \to 0$ and therefore the Richardson's scheme of calculation is consistent. In addition, this side goes to zero as the second power of Δt and the second power of Δx, implying that the scheme is of second order accuracy in both time and space as well. Indeed, this result further verifies what would otherwise be expected because the way this scheme is based on Taylor series expansions.

We furthermore provide here the evolution equation with only space derivatives, i.e. the modified equation. In order to achieve it, we firstly find expressions for $\frac{\partial^3 T}{\partial t^3}$, and secondly (be careful with this) for $\frac{\partial^3 T}{\partial x^2 \partial t}$ and $\frac{\partial^3 T}{\partial x \partial t^2}$, by differentiating Eq. (2.3); all of which we use systematically to eliminate the time derivatives in it. This implies that the modified equation associated with the Richardson's scheme, the equation of the grid function from Richardson's difference equation, is:

$$\frac{\partial T}{\partial t} + v\frac{\partial T}{\partial x} = \frac{1}{6}(-C + C^3)\frac{(\Delta x)^3}{\Delta t}\frac{\partial^3 T}{\partial x^3} + \mathcal{O}((\Delta x)^4), \tag{2.4}$$

which is one of two ways to next not only calculate the local error but also estimate the stability (see below).

2.1.3. **Stability.** We secondly analyze the stability using the von Neumann's method. Substituting a term of Eq. (2.1) of Part I into each term in Eq. (2.1) we get the equation for the growth factor (Eq. (2.15) of Part I),

$$G = \frac{1}{G} - C\,(e^{-i\,k\,\Delta x} - e^{i\,k\Delta x}) = \frac{1}{G} + 2\,i\,C\sin{(k\Delta x)}, \tag{2.5}$$

whose complex solutions are

$$G_{\pm} = \pm\sqrt{1 - [C\,\sin{(k\Delta x)}]^2} - i\,C\,\sin{(k\Delta x)}. \tag{2.6}$$

That is to say, given its nature of three time levels, in a given instant each real valued growth factor associated with the Richardson's scheme has two temporal modes present in the numerical solution. In other words, as a three time level that it is, this scheme has two temporal modes. Note, the solution G_+ corresponds to the physical mode because for well

resolved components ($k\Delta x \ll 1$) its real (observable) part is as it should be; and viceversa:

$$\lim_{k\Delta x \to 0} \Re(G_{\pm}) = \pm 1. \tag{2.7}$$

Here, concerning stability, the growth factor magnitudes are such that

(1) either the radical in Eq. (2.7) is negative, i.e. $C > 1$ which implies $|G_{+}| \geq 1$, which does not satisfy Eq. (2.16) of Part I and thus the scheme is unstable;
(2) or the radical in Eq. (2.7) is positive, i.e. $C^2 \leq 1$ which implies $|G_{\pm}| = 1$, satisfying stability criterion.

Therefore, the Richardson's scheme is neutrally stable,

$$|G_{\pm}| = 1, \tag{2.8}$$

i.e. the amplitudes of the Fourier components neither increases nor decrease as time evolves which is a desirable property because is in line with the lack of diffusion of the general analytical solution (Eq. (2.18) of Part I), only if we restrict to the so-called (after its discoverers [7]) Courant-Friedrichs-Lewy condition for the explicit numerical solutions of hyperbolic partial differential equations:

$$C \leq 1, \tag{2.9}$$

which, like the Courant-Friedrichs-Lewy-type condition in parabolic partial differential equations, provides critical information about the number of discretization points over the wave length to be selected. In particular, this inequality states that because the explicit schemes use information from the previous time step to find the solution of the present time step it is hence necessary to use a small specific time step size. On the other hand, because the implicit schemes majorly use information from neighboring points of the current time step to find the solution it is hence viable to use a large time step size. However, the physical interpretation of the Courant-Friedrichs-Lewy condition in hyperbolic partial differential equations, Eq. (2.9), is quite different from that of the Courant-Friedrichs-Lewy-type condition in parabolic partial differential equations, $F \leq 0.5$, as mentioned in Part I. In a superficial way, Eq. (2.9) is interpreted as a condition which constraints the grid speed to be greater than the advection speed. We revise this interpretation below.

Alternatively, the modified equation is another way to obtain this. The first (odd) term on the right hand of Eq. (2.4), which acts as a dispersive term, has to be positive for T_j^n not to be propagated in the opposite direction; i.e. has to be $C \leq 1$, as we have just obtained.

2.1.4. **Accuracy.** We thirdly investigate how accurate, both in magnitude and in phase, the numerical solution is using the Hirt's and von Neumann's complementary analysis.

On the one hand, by applying the discrete Fourier series grid solution of Eq. (2.1) of Part I to the Richardson's modified equation 2.4 we see that there is only odd-order derivatives, implying the damping term of the numerical solution is clearly unity (see Eq. (2.27) of Part I) which is shown in left panel of Fig. 1.

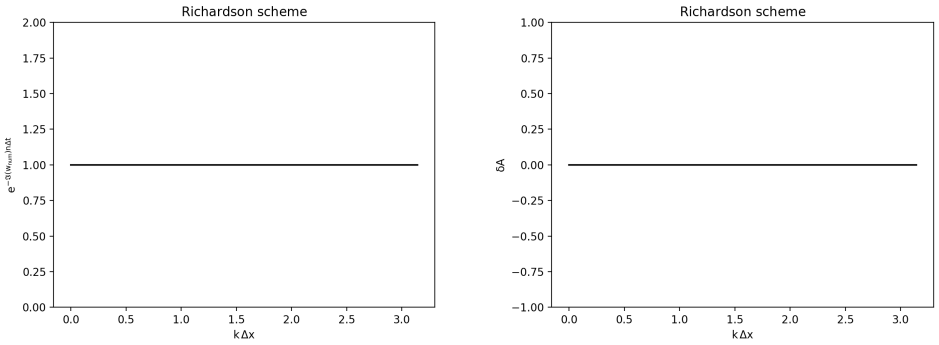

FIGURE 1. Damping factor and relative amplitude error as a function of phase angle or frequency, in radians, for specific C number values.

Alternatively, since the exact growth factor is equal to unity, the relative amplitude error (Eq. (2.29) of Part I) is given by

$$\delta A = 0, \tag{2.10}$$

as shown in right panel of Fig. 1.

On the other hand, by applying the discrete Fourier series grid solution of Eq. (2.1) of Part I to the Richardson's modified equation (2.4) truncated up to the five-order derivatives, then we see that the dispersive term is given by

$$\exp\left\{i\,k\,\left[x - v\,t + \frac{1}{6}(C - C^3)\,\frac{(\Delta x)^3}{\Delta t}\,k^2\,t\right]\right\}, \tag{2.11}$$

implying the dispersive phase velocity shown in Fig. 2. We find a numerical propagation speed smaller than the physical one, but shifting closer to the physical one with increasing C's. This leads to the striking fact that the instantaneous velocity flips sign once a instability-threshold is

reached, when the numerical speed reaches exact value. More on this later.

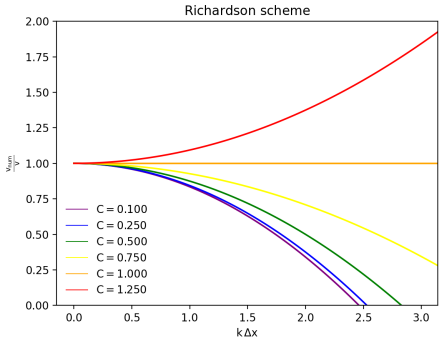

FIGURE 2. The phase velocity of the Richardson's solution (approximated to the five-order derivatives), Eq. (2.11) vs. frequency in radians, for specific C values which are distinguished by line colors.

Alternatively, from the von Neumann's complementary analysis point of view, each discrete Fourier component that is a solution to the Richardson's scheme (see Eq. (2.1) of Part I for the full series which is the sum over all the possible wave numbers) is a linear combination of the two wave solutions contained in the growth factor, Eq. (2.7), with magnitude components given by Eq. (2.8) and with the numerical phase components of each of these two modes given by

$$\phi_{\pm} = \arctan\left(\frac{\Im(G_{\pm})}{\Re(G_{\pm})}\right) = \arctan\left(\frac{-C\sin(k\Delta x)}{\pm\sqrt{1-[C\,\sin(k\Delta x)]^2}}\right), \tag{2.12}$$

which we show in the upper panels of the Fig. 3, finding that they are such that verify the relationship $\phi_+ + \phi_- = -\pi$. Hence, the Richardson's numerical solution in space and time for each Fourier mode becomes

$$\begin{aligned} T_j^n &= (c_1\, e^{i\,\phi_+\, n\Delta t} + c_2\, e^{i\,(\pi+\phi_+)\, n\Delta t})\, e^{i\,k\,j\Delta x} \\ &= (c_1\, e^{i\,\phi_+\, n\Delta t} + (-1)^n\, c_2\, e^{i\,\phi_+\, n\Delta t})\, e^{i\,k\,j\Delta x}, \end{aligned} \tag{2.13}$$

i.e. the second term alternates signs in each time step, is therefore unphysical or false and generates instabilities. This is a interesting but undesirable behavior which is caused because the Richardson's scheme is a three time level scheme. In fact, we found a similar behavior using the Du Fort-Frankel scheme in Part I.

Therefore, since the exact phase speed is the $-v$, we present in lower panels of the Fig. 3 the physical and computational relative phase errors (see Eq. (2.30) of Part I) of the Richardson's scheme plotted against the phase angle for specific C values.

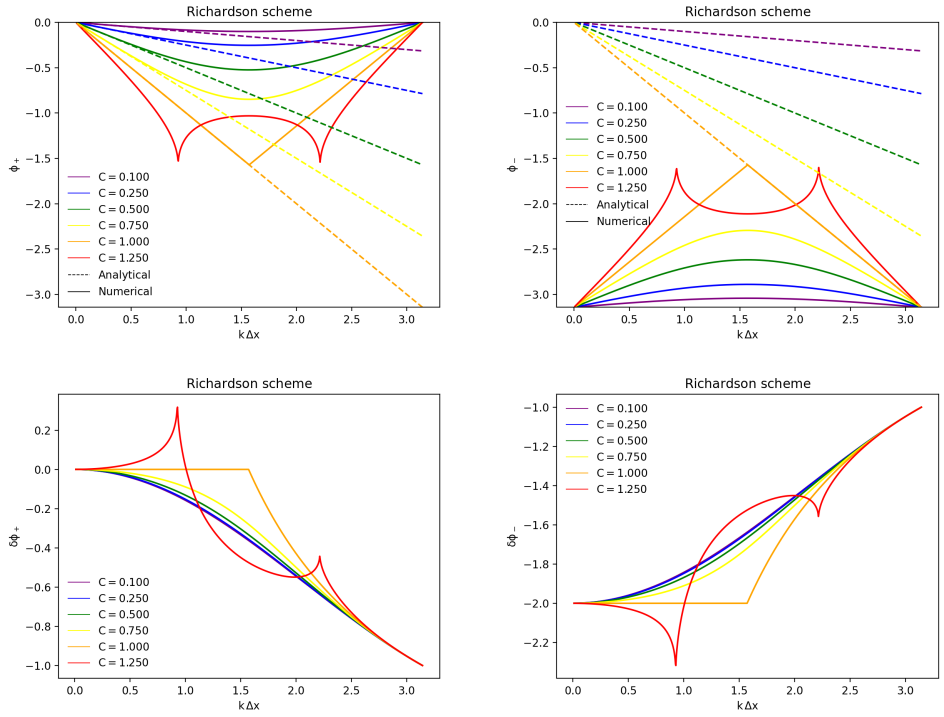

FIGURE 3. Upper: the numerical phase components of G_+ and G_-, respectively. In an Argand diagram G_+ is in the fourth quadrant and G_- is in the third quadrant (n.b., Eq. (2.12)). Lower: the physical (left panel) and computational (right panel) relative phase errors as a function of phase angle or frequency, in radians, for specific C number values.

Examining the left panels in Fig. 3 referring to the physical waves, we can see that although both low and high frequency harmonics are nearly stationary, the mid oscillatory waves are propagated with different speeds, implying that the Richardson's scheme is selectively dispersive. Specifically, this implies that whilst the low frequency physical (numerical) waves are well resolved, those with high frequency will be poorly resolved ($\delta\phi \simeq -1$ in the right panel). The same is true for the the

extra solution, the computational (numerical) waves showed in the right panels in Fig. 3, propagating in opposite direction as we deduce from these panels. Furthermore, we observe in Fig. 3 (see, e.g., the left panels referring to the physical waves), in agreement with Fig. 2, that for $C < 1$ the physical waves have leading shift, $\delta\phi < 0$ (see especially the lower panels of Fig. 7), indicating a numerical propagation speed smaller than the physical one; but shift closer to the line $\delta\phi = 0$ once the stability threshold is reached, when the relative phase shift error flips sign and the Fourier modes will have lagging shift (see red line in Fig. 3). Finally, Fig. 3 also shows us that in the remaining case, $C = 1$, the Richardson's scheme is exact (remembering Fig. 1). Indeed, in this case we deduce that Eq. (2.1) reduces to $T_j^{n+1} = T_{j-1}^n$, since along characteristics $T_j^{n-1} = T_{j+1}^n$ (see A); i.e., in this case the even and odd time steps are not decoupled and do not split apart. However, this does not mean that there is no moderate oscillations from the linear combination of the two left and right panels of the Fig. 3 corresponding to the physical and computational modes, respectively; which increase as the time progresses.

2.1.5. **Monotonicity.** Finally, Eq. (2.1) violates the condition for preserving monotonicity (Eq. (2.31) of Part I) since the term T_{j+1}^n has a coefficient $-C < 0$. That is, the Richardson's scheme is nonmonotone. Hence, it also may produce additional spurious oscillations.

2.2. The Schmidt's 1924 single-step explicit scheme.

2.2.1. **Construction.** In 1924 Schmidt [8] proposed a second order approximation for the spatial derivative but forward in time, i.e.

$$\frac{T_j^{n+1} - T_j^n}{\Delta t} = -v\frac{T_{j+1}^n - T_{j-1}^n}{2\Delta x}, \tag{2.14}$$

which is also reformulated in Table 1 using Eq. (2.2). In this way he was able to avoid the initial value issue that the Richardson's scheme applied to the linear differential equation had, i.e. this scheme is a one-step, explicit scheme.

2.2.2. **Consistency and order of accuracy.** We firstly analyze the consistency of the scheme using the Hirt's method. Substituting each value of the grid function at points other than point (x_j, t^n) in the scheme

in a Taylor series around the value T_j^n at that point (x_j, t^n), i.e. substituting Eqs. 2.6, 2.12 and 2.13 of Part I in Eq. (2.14), gives

$$\frac{\partial T}{\partial t} + v\frac{\partial T}{\partial x} = -\frac{(\Delta t)}{2}\frac{\partial^2 T}{\partial t^2} - \frac{v\,(\Delta x)^2}{6}\frac{\partial^3 T}{\partial x^3} - \frac{(\Delta t)^2}{6}\frac{\partial^3 T}{\partial t^3} + \cdots . \quad (2.15)$$

We then see from that equation, which is not yet the modified equation, that its right hand side vanishes when $\Delta t \to 0$ and $\Delta x \to 0$ and therefore the Schmidt's scheme of calculation is consistent. In addition, this side goes to zero as the first power of Δt and the second power of Δx, implying that the scheme is of first order accuracy in time and second order accuracy in space as well. Indeed, this result further verifies what would otherwise be expected by construction because the way this scheme is based on Taylor series expansions.

We furthermore provide here the evolution equation with only space derivatives, i.e. the modified equation. In order to achieve it, we firstly find expressions for $\frac{\partial^2 T}{\partial t^2}$ and $\frac{\partial^3 T}{\partial t^3}$, and secondly (be careful with this) for $\frac{\partial^3 T}{\partial x^2 \partial t}$ and $\frac{\partial^3 T}{\partial x \partial t^2}$, by differentiating Eq. (2.15); all of which we use systematically to eliminate the time derivatives in it. This implies that the modified equation associated with the Schmidt's scheme, the equation of the grid function from Schmidt's difference equation, is:

$$\frac{\partial T}{\partial t} + v\frac{\partial T}{\partial x} = \frac{1}{2}(-C^2)\frac{(\Delta x)^2}{\Delta t}\frac{\partial^2 T}{\partial x^2} + \frac{1}{6}(-C - 2\,C^3)\frac{(\Delta x)^3}{\Delta t}\frac{\partial^3 T}{\partial x^3} + \mathcal{O}((\Delta x)^3), \quad (2.16)$$

which is one of two ways to next not only calculate the local error but also estimate the stability (see below). So far so good.

2.2.3. **Stability.** We secondly analyze the stability using the von Neumann's method. Substituting a term of Eq. (2.1) of Part I into each term in Eq. (2.14) we get the complex valued growth factor (Eq. (2.15) of Part I) associated with the Schmidt's scheme,

$$G = 1 - \frac{1}{2}C\,(e^{i\,k\,\Delta x} - e^{-i\,k\Delta x}) = 1 - i\,C\sin(k\Delta x), \quad (2.17)$$

whose magnitude component takes the form

$$|G| = \sqrt{1 + (C\sin(k\Delta x))^2}, \quad (2.18)$$

which does not satisfy Eq. (2.16) of Part I and thus the scheme is unstable for the advection equation, as shown in Fig. 4 where we find that the relative dissipation error (Eq. (2.29) of Part I) is higher to 0. Hence, and because of its enormous simplicity, the Schmidt's scheme may be used just to initiate the Richardson's scheme.

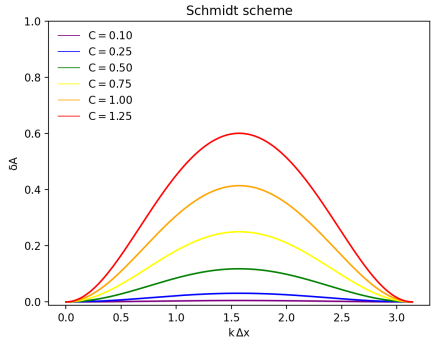

FIGURE 4. Relative amplitude error as a function of phase angle or frequency, in radians, for specific Courant number values.

Alternatively, the modified equation is another way to obtain this. The first (even) term on the right hand of Eq. (2.16), which acts as a diffusive term, has to be positive for T_j^n to be decayed; i.e. has to be $C^2 \leq 0$, which is impossible; implying Schmidt's T_j^{n+1} grows and become dissipatively unstable/unbounded, confirming Eq. (2.18).

So that is all on the application of the Schmidt's scheme to advection equations.

2.3. **The Crank-Nicolson 1947 single-step semi-explicit scheme.**

2.3.1. **Construction.** In 1947 Crank and Nicolson [9] achieved a forward in time scheme using, to say the least, the average of the scheme formerly proposed by Schmidt and the Laasonen's scheme described below. Hence, this scheme is not based on Taylor series expansions, implying that we do not know apriori whether the consistency requirement is satisfied or not. In this way they obtained the scheme:

$$\frac{T_j^{n+1} - T_j^n}{\Delta t} = -v\,\frac{1}{2}\left(\frac{T_{j+1}^{n+1} - T_{j-1}^{n+1}}{2\Delta x} + \frac{T_{j+1}^{n} - T_{j-1}^{n}}{2\Delta x}\right), \tag{2.19}$$

which is again reformulated in Table 1 using Eq. (2.2).

This is also a one step scheme. However, as a scheme that does not proceed in a hierarchical, bottom-up fashion, the Crank-Nicolson scheme gives a (tridiagonal) system of equations to solve for all the values of T_i^{n+1} simultaneously and we must to resort to standard matrix equation solvers (e.g., see [10]), which is complicated to implement for parallel

execution. Specifically, the Crank-Nicolson scheme will be referred to as a semi-explicit scheme since T_j^{n+1} depends also on data at next time level. Besides, this monolithic nature of several much-used nonexplicit schemes implies that any anomaly strongly affects the entire solution; which, depending on the initial conditions, is not necessarily one more attractive feature for diffusion (see next Section).

2.3.2. **Consistency and order of accuracy.** Eq. (2.19) now poses a significant challenge to deriving consistency because we must reduce the number of indexes in it before raising and/or lowering them. Thus, in this situation we reformulate Eq. (2.19) once more so it would be suitable to derive an equation with derivatives only. Specifically, we rewrite Eq. (2.19) as $T_j^{n+1} = T_j^n + 0.5\,C\,T_{j-1}^{n+1/2} - 0.5\,C\,T_{j+1}^{n+1/2}$. Next, substituting each value of T at points other than point $(x_j, t^{n+1/2})$ in this equation in a Taylor series around the value T_j^n at that point $(x_j, t^{n+1/2})$, gives

$$\frac{\partial T}{\partial t} + v\frac{\partial T}{\partial x} = -\frac{v\,(\Delta x)^2}{6}\frac{\partial^3 T}{\partial x^3} - \frac{(\Delta t)^2}{24}\frac{\partial^3 T}{\partial t^3} + \cdots . \tag{2.20}$$

We then see from that equation, which is not yet the modified equation, that the right hand side vanishes when $\Delta t \to 0$ and $\Delta x \to 0$ and therefore the Crank-Nicolson scheme of calculation is consistent. In addition, this side goes to zero as the second power of Δt and the second power of Δx, implying that the scheme is of second order accuracy in both time and space.

We furthermore provide here the evolution equation with only space derivatives, i.e. the modified equation. In order to achieve it, we firstly find expressions for $\frac{\partial^2 T}{\partial t^2}$ and $\frac{\partial^3 T}{\partial t^3}$, and secondly (be careful with this) for $\frac{\partial^2 T}{\partial x \partial t}$ and $\frac{\partial^3 T}{\partial x^2 \partial t}$, by differentiating Eq. (2.20); all of which we use systematically to eliminate the time derivatives in it. This implies that the modified equation associated with the Crank-Nicolson scheme, the equation of the grid function from Crank-Nicolson difference equation, is:

$$\frac{\partial T}{\partial t} + v\frac{\partial T}{\partial x} = \frac{1}{24}(-4\,C - 2\,C^3)\frac{(\Delta x)^3}{\Delta t}\frac{\partial^3 T}{\partial x^3} + \mathcal{O}((\Delta x)^3), \tag{2.21}$$

which is one of two ways to next not only calculate the local error but also estimate the stability.

2.3.3. **Stability.** We secondly now analyze the stability using the von Neumann's method. Substituting a term of Eq. (2.1) of Part I into each

term in Eq. (2.19) we get the following complex valued, growth factor associated with the Crank-Nicolson scheme:

$$G = \frac{1 - i\,\frac{C}{2}\sin(k\Delta x)}{1 + i\,\frac{C}{2}\sin(k\Delta x)} = 1, \tag{2.22}$$

i.e. the amplitudes of the Fourier components neither increases nor decrease as time evolves, which is a desirable property because is in line with the lack of diffusion of the general analytical solution (Eq. (2.18) of Part I). Hence, the Crank-Nicolson scheme is stable even at large time step size, although (be careful with this) this will not necessarily give accurate solution. This is because, the non-explicit schemes use the information from neighboring cell of the current time step to find the solution.

Alternatively, the Hirt's method is another way to obtain this. The even, first term on the right hand of modified equation Eq. (2.21), which acts as a dispersive term (is an odd-order derivative), is always negative and also there is no diffusive derivatives implying that the Crank-Nicolson scheme is indeed neutrally stable.

2.3.4. **Accuracy.** We thirdly investigate how accurate, both in magnitude and in phase, the numerical solution is using the Hirt's and von Neumann's complementary analysis.

On the one hand, by applying the discrete Fourier series grid solution of Eq. (2.1) of Part I to the Crank-Nicolson modified equation (2.21) we see that there is only odd-order derivatives, implying the damping term of the numerical solution is clearly unity (see Eq. (2.27) of Part I) which is shown in left panel of Fig. 5.

Alternatively, since the exact growth factor is equal to unity, the relative amplitude error (Eq. (2.29) of Part I) is given by

$$\delta A = 0, \tag{2.23}$$

as shown in right panel of Fig. 5. The same as the Richardson's scheme.

On the other hand, by applying the discrete Fourier series grid solution of Eq. (2.1) of Part I to the Crank-Nicolson modified equation (2.21) truncated up to the five-order derivatives, then we see that the dispersive term is given by

$$\exp\left\{i\,k\,\left[x - v\,t + \frac{1}{24}(4\,C + 2\,C^3)\,\frac{(\Delta x)^3}{\Delta t}\,k^2\,t\right]\right\}, \tag{2.24}$$

implying the dispersive phase velocity shown in Fig. 6. We now find a numerical propagation speed smaller than the physical one, but shifting away from the physical one with increasing C's. This leads to the fact

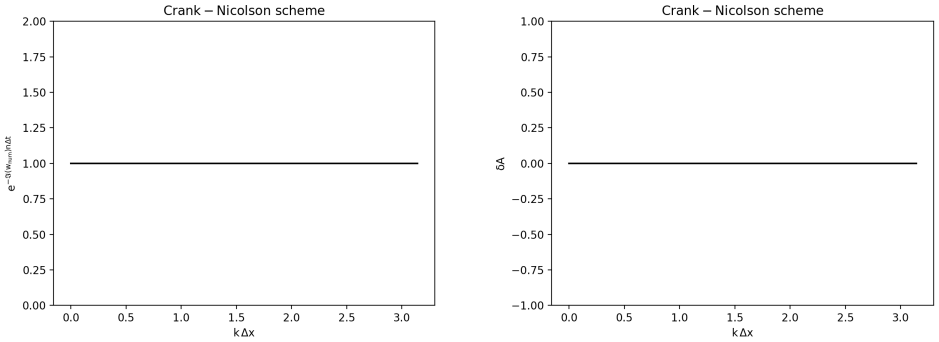

FIGURE 5. Damping factor and relative amplitude error as a function of phase angle or frequency, in radians, for specific C number values.

that the instantaneous velocity does not flip sign because the numerical speed never reaches exact value, implying the Crank-Nicolson scheme don't have instability issue. More on this later.

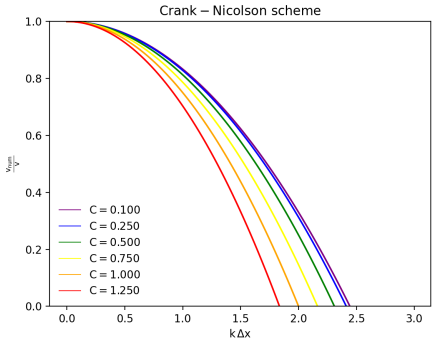

FIGURE 6. The phase velocity of the Crank-Nicolson solution (approximated to the five-order derivatives), Eq. (2.24) vs. frequency in radians, for specific C values which are distinguished by line colors.

Alternatively, from the von Neumann's complementary analysis point of view, the numerical phase component of the Crank-Nicolson growth factor, Eq. (2.22), is given by

$$\phi = \arctan\left(\frac{\Im(G)}{\Re(G)}\right) = \arctan\left(\frac{-C\sin(k\Delta x)}{1-\left(\frac{C}{2}\sin(k\Delta x)\right)^2}\right), \tag{2.25}$$

which we show in the left panel of the Fig. 7.

Therefore, since the exact phase speed is the $-v$, we present in the right panel of the Fig. 7 the numerical relative phase error (see Eq. (2.30) of Part I) of the Crank-Nicolson scheme plotted against the phase angle for specific C values.

Examining the phase component of the scheme for the resolvable wave number components of the numerical solution, Fig. 7, we can again see that although both low and high frequency harmonics are nearly stationary, the mid oscillatory waves are propagated with different speeds, implying that the Crank-Nicolson scheme is also selectively dispersive. Specifically, this implies that whilst the low frequency waves are well resolved, those with high frequency will be poorly resolved ($\delta\phi \simeq -1$ in the right panel). Also, for all values of C we have leading shift, the relative phase error is less than 0 (see the right panel of Fig. 7), indicating a numerical propagation speed smaller than the physical one; but shift away from the line $\delta\phi = 0$ or the physical speed (see the left panel), implying the Crank-Nicolson scheme don't have instability issue. Finally, Fig. 7 (especially its right panel) also shows us that relative phase is very little affected by the value of C.

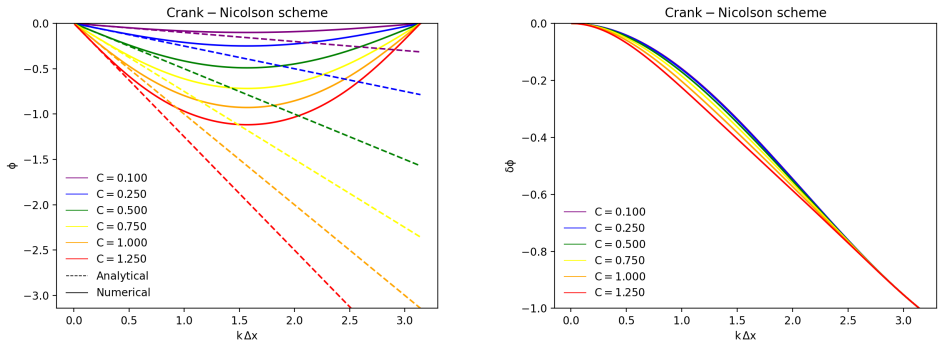

FIGURE 7. Left: the numerical phase component. Right: the numerical relative phase error as a function of phase angle or frequency, in radians, for specific C number values.

2.3.5. **Monotonicity.** Finally, from the Eq. (2.19) the coefficients of the new solution are 1, $\frac{C}{4}$ and $-\frac{C}{4}$. That way, the Crank and Nicolson scheme is nonmonotone. Hence, it also may produce additional spurious oscillations.

2.4. **The Laasonen's 1949 single-step implicit scheme.**

2.4.1. **Construction.** In 1949 Laasonen [11] used the same approximation as Schmidt did, but evaluating the space derivative forwards in time, at time step $n+1$ instead of at time step n; i.e.,

$$\frac{T_j^{n+1}-T_j^n}{\Delta t}=-v\frac{T_{j+1}^{n+1}-T_{j-1}^{n+1}}{2\Delta x}. \tag{2.26}$$

Table 1 emphasizes that Eq. (2.26) is purely time-implicit. Therefore, as a non-explicit scheme that it is, the solution at the next time level is computed from the present time level by solving the tridiagonal system of equations that Eq. (2.26) gives (e.g., see [10]). The same as the Crank-Nicolson scheme.

2.4.2. **Consistency and order of accuracy.** We firstly analyze the consistency of the scheme using the Hirt's method. Substituting each value of T at points other than point (x_j,t^{n+1}) in the scheme in a Taylor series around the value T_j^{n+1} at that point (x_j,t^{n+1}), i.e. we substitute Eqs. 2.6, 2.12 and 2.13 of Part I in Eq. (2.26), gives

$$\frac{\partial T}{\partial t}+v\frac{\partial T}{\partial x}=\frac{\Delta t}{2}\frac{\partial^2 T}{\partial t^2}-\frac{v\,(\Delta x)^2}{3}\frac{\partial^3 T}{\partial x^3}-\frac{(\Delta t)^2}{6}\frac{\partial^3 T}{\partial t^3}+\cdots. \tag{2.27}$$

We then see from that equation, which is not yet the modified equation, that the right hand side vanishes when $\Delta t\to 0$ and $\Delta x\to 0$ and therefore the Laasonen's scheme of calculation is consistent. In addition, this side goes to zero as the first power of Δt and the second power of Δx, implying that the scheme is of first order accuracy in time and second order accuracy in space as well. Indeed, this result further verifies what would otherwise be expected because the way this scheme is based on Taylor series expansions.

We furthermore provide here the evolution equation with only space derivatives, i.e. the modified equation. In order to achieve it, we firstly find expressions for $\frac{\partial^2 T}{\partial t^2}$, and secondly (be careful with this) for $\frac{\partial^3 T}{\partial t^3}$, $\frac{\partial^2 T}{\partial x\partial t}$ and $\frac{\partial^3 T}{\partial x^2\partial t}$, by differentiating Eq. (2.27); all of which we use systematically to eliminate the time derivatives in it. This implies that the modified equation associated with the Laasonen's scheme, the equation of the grid function from Laasonen's difference equation, is:

$$\frac{\partial T}{\partial t}+v\frac{\partial T}{\partial x}$$

$$= \frac{C^2}{2}\frac{(\Delta x)^2}{\Delta t}\frac{\partial^2 T}{\partial x^2} - \left(\frac{C+2\,C^3}{6}\right)\frac{(\Delta x)^3}{\Delta t}\frac{\partial^3 T}{\partial x^3} + \frac{C^2}{12}\frac{(\Delta x)^4}{\Delta t}\frac{\partial^4 T}{\partial x^4} + \mathcal{O}((\Delta x)^4), \tag{2.28}$$

which is one of two ways to next not only calculate the local error but also estimate the stability.

2.4.3. **Stability.** We secondly now analyze the stability using the von Neumann's method. Substituting a term of Eq. (2.1) of Part I into each term a term in Eq. (2.26) we get the following complex valued, growth factor associated with the Laasonen's scheme:

$$G = \frac{1}{1 + i\,C\sin(k\Delta x)} = \frac{1 - i\,C\sin(k\Delta x)}{1 + C^2\sin^2(k\Delta x)}, \tag{2.29}$$

whose magnitude component takes the form

$$|G| = \frac{\sqrt{1 + C^2\sin^2(k\Delta x)}}{1 + C\sin(k\Delta x)} < 1, \tag{2.30}$$

which satisfies Eq. (2.16) of Part I and thus the Laasonen's scheme is stable for the advection equation.

Alternatively, the modified equation is another way to obtain this. The first (even) term on the right hand of Eq. (2.28), which acts as a diffusion term, always is positive implying that the Laasonen's scheme is indeed unconditionally stable.

In fact, this property of being stable turns out to be true for all purely implicit schemes. That said, if not for stability, for accuracy we cannot use a large time step. To clearly see it, note the ratio of the Laasonen's numerical damping rate (from Eq. (2.28) of Part I, $e^{-iw_{num}\Delta t} = |G|$) to the exact damping rate (the unity) is

$$\frac{w_{num}}{w} = \ln\left(\frac{\sqrt{1 + C^2\sin^2(k\Delta x)}}{1 + C\sin(k\Delta x)}\right) = -C\,(k\Delta x) + C^2(k\Delta x)^2 + \mathcal{O}((k\Delta x)^3); \tag{2.31}$$

which show us that for, e.g., $C = 1$ the error on the damping rate is as much as about the exact damping rate (Eq. (2.31) is on average about 1).

2.4.4. **Accuracy.** We thirdly investigate how accurate, both in magnitude and in phase, the numerical solution is using the Hirt's and von Neumann's complementary analysis.

On the one hand, by applying the discrete Fourier series grid solution of Eq. (2.1) of Part I to the Laasonen's modified equation (2.28) truncated up to the five-order derivatives we see that the damping term of the numerical solution is not unity as it should be but it is given by

$$\exp\left[-\frac{C^2}{2}\,\frac{(\Delta x)^2}{\Delta t}\,k^2\,\Delta t+\frac{C^2}{12}\,\frac{(\Delta x)^4}{\Delta t}\,k^4\,\Delta t\right], \tag{2.32}$$

which is shown in left panel of Fig. 8.

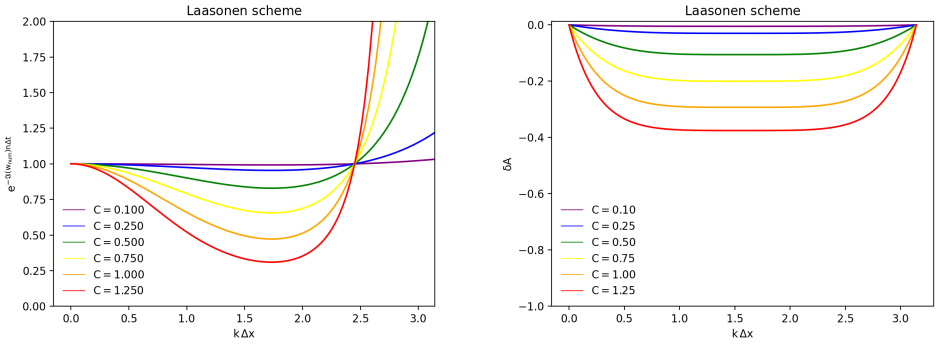

FIGURE 8. Damping factor (approximated to the five-order derivatives) and relative amplitude error as a function of phase angle or frequency, in radians, for specific C number values. We conclude that the damping factor offers an average description of evolutionary behaviors of amplitudes that is valid at least qualitatively.

We naturally notice that there is no dissipation for $k = 0$ and it will be greater for larger values of k, i.e. at higher wavenumbers. Also the Hirt analysis illustrates that dispersion of this scheme (in fact, almost always) is one order of magnitude smaller than its dissipation.

Alternatively, since the exact growth factor is equal to unity, the relative amplitude error (Eq. (2.29) of Part I) is given by

$$\delta A=\frac{\sqrt{1+C^2\sin^2(k\Delta x)}}{1+C\sin(k\Delta x)}-1, \tag{2.33}$$

and is shown in right panel of Fig. 8 where we find, in agreement with the left panel remembering this is obtaining by truncating the numerical solution up to the five-order derivatives, that it both decreases rapidly a little from 0 at $k\Delta x = 0$ (for consistency reasons) and increases rapidly

to 0 again at $k\Delta x = \pi$; i.e. the Laasonen's scheme is not uniformly dissipative, although its effect is not too great but relatively weak.

On the other hand, by applying the discrete Fourier series grid solution of Eq. (2.1) of Part I to the Laasonen's modified equation (2.28) truncated up to the five-order derivatives, then we see that the dispersive term is given by

$$\exp\left\{i\,k\,\left[x - v\,t + \frac{1}{6}(C + 2\,C^3)\frac{(\Delta x)^3}{\Delta t}\,k^2\,t\right]\right\}, \tag{2.34}$$

implying the dispersive phase velocity shown in Fig. 9. We find a numerical propagation speed smaller than the physical one, but moving away from the physical one with increasing C's. This leads to the fact that the instantaneous velocity does not flip sign because the numerical speed never reaches exact value, implying the Laasonen's scheme don't have instability issue. More on this later.

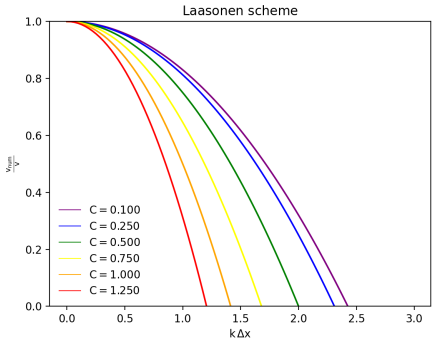

FIGURE 9. The phase velocity of the Laasonen's solution (approximated to the five-order derivatives), Eq. (2.34) vs. frequency in radians, for specific C values which are distinguished by line colors.

Alternatively, from the von Neumann's complementary analysis point of view, the numerical phase component of the Laasonen's growth factor, Eq. (2.29), is given by

$$\phi = \arctan\left(\frac{\Im(G)}{\Re(G)}\right) = \arctan\left[-C\sin\left(k\Delta x\right)\right], \tag{2.35}$$

which we show in the left panel of the Fig. 10.

Therefore, since the exact phase speed is the $-v$, we present in the right panel of the Fig. 10 the numerical relative phase error (see Eq.

(2.30) of Part I) of the Laasonen's scheme plotted against the phase angle for specific C values.

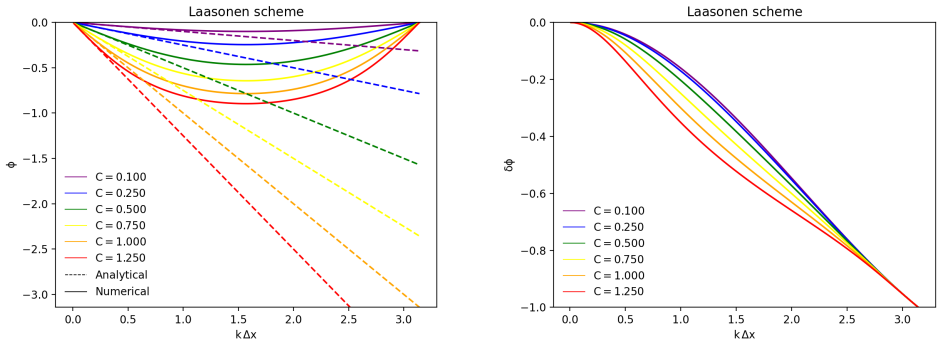

FIGURE 10. Left: the numerical phase component. Right: the numerical relative phase error as a function of phase angle or frequency, in radians, for specific C number values.

We find that the (dispersive) behavior is similar to that using the Crank-Nicolson scheme. Indeed, the left panel of Fig. 10 shows us that for all values of C we have leading shift, the relative phase error is less than 0 (see the left panel of Fig. 10), indicating a numerical propagation speed smaller than the physical one; but shift away from the line $\delta\phi = 0$, implying again the Laasonen's scheme don't have instability issue, either. However, let's not forget that the Laasonen's dissipative behavior is much worse than that using the Crank-Nicolson scheme.

2.4.5. **Monotonicity.** The Laasonen's scheme is an implicit scheme. Since T_j^{n+1} depends only on T_j^n, then we cannot use the convex combination technique. Therefore we must demonstrate Eq. (2.31) of Part I. From Eq. (2.26) (see Table 1) we also get

$$-0.5\,C\,T_{j-2}^{n+1} + T_{j-1}^{n+1} + 0.5\,C\,T_j^{n+1} = T_{j-1}^n, \tag{2.36}$$

which subtracted from Eq. (2.26) gives

$$T_j^{n+1} - T_{j-1}^{n+1} = T_j^n - T_{j-1}^n - 0.5\,C\,(T_{j+1}^{n+1} - T_j^{n+1}) + 0.5\,C\,(T_{j-1}^{n+1} - T_{j-2}^{n+1}), \tag{2.37}$$

and if in this equation we take the absolute value of both sides, use the triangle inequality on the right-side and sum the two sides over all j then we get Eq. (2.31) of Part I. Hence, the Laasonen's scheme is monotone and does not introduce oscillations.

2.5. **The Courant-Isaacson-Rees 1952 single-step explicit scheme.**

2.5.1. **Construction.** In 1952 Courant, Isaacson and Rees [12] used the forward in time approximation, Eq. (2.6) of Part I, to replace the time rate of change and the one-sided in the correct direction Eq. (2.10) of Part I for the first order derivative in space. In this way they obtained the following one-step, explicit scheme:

$$\frac{T_j^{n+1} - T_j^n}{\Delta t} = -v \frac{T_j^n - T_{j-1}^n}{\Delta x}, \tag{2.38}$$

which is reformulated in Table 1 using Eq. (2.2).

2.5.2. **Consistency and order of accuracy.** We firstly analyze the consistency of the scheme using the Hirt's method. Substituting each value of T at points other than point (x_j, t^n) in the scheme in a Taylor series around the value T_j^n at that point (x_j, t^n), i.e. we substitute Eqs. 2.6 and 2.13 of Part I in Eq. (2.38), gives

$$\frac{\partial T}{\partial t} + v\frac{\partial T}{\partial x} = \frac{v\,\Delta x}{2}\frac{\partial^2 T}{\partial x^2} - \frac{\Delta t}{2}\frac{\partial^2 T}{\partial t^2} - \frac{v\,(\Delta x)^2}{6}\frac{\partial^3 T}{\partial x^3} - \frac{(\Delta t)^2}{6}\frac{\partial^3 T}{\partial t^3} + \cdots . \tag{2.39}$$

We then see from that equation, which is not yet the modified equation, that the right hand side vanishes when $\Delta t \to 0$ and $\Delta x \to 0$ and therefore the Courant-Isaacson-Rees scheme of calculation is consistent. In addition, this side goes to zero as the first power of Δt and the first power of Δx, implying that the scheme is of first order accuracy in both time and space as well. Indeed, this result further verifies what would otherwise be expected because the way this scheme is based on Taylor series expansions.

We furthermore provide here the evolution equation with only space derivatives, i.e. the modified equation. In order to achieve it, we firstly find expressions for $\frac{\partial^2 T}{\partial t^2}$ and $\frac{\partial^3 T}{\partial t^3}$, and secondly (be careful with this) for $\frac{\partial^2 T}{\partial x \partial t}$, $\frac{\partial^3 T}{\partial x^2 \partial t}$ and $\frac{\partial^3 T}{\partial x \partial t^2}$, by differentiating Eq. (2.39); all of which we use systematically to eliminate the time derivatives in it. This implies that the modified equation associated with the Courant-Isaacson-Rees scheme, the equation of the grid function from Courant-Isaacson-Rees difference equation, is:

$$\frac{\partial T}{\partial t} + v\frac{\partial T}{\partial x}$$

$$= \frac{C - C^2}{2} \frac{(\Delta x)^2}{\Delta t} \frac{\partial^2 T}{\partial x^2} + \left(\frac{-C + 3\,C^2 - 2\,C^3}{6} \right) \frac{(\Delta x)^3}{\Delta t} \frac{\partial^3 T}{\partial x^3} + \mathcal{O}((\Delta x)^4), \tag{2.40}$$

which is one of two ways to next not only calculate the local error but also estimate the stability.

2.5.3. **Stability.** We secondly now analyze the stability using the von Neumann's method. Substituting a term of Eq. (2.1) of Part I into each term a term in Eq. (2.38) we get the following complex valued, growth factor associated with the Courant-Isaacson-Rees scheme:

$$G = 1 - C + C\, e^{i\,k\,\Delta x} = 1 - C[1 - \cos(k\Delta x)] - i\,C \sin(k\Delta x), \tag{2.41}$$

whose magnitude component takes the form

$$|G| = \sqrt{1 - 2C(1 - C)[1 - \cos(k\Delta x)]}, \tag{2.42}$$

which satisfies Eq. (2.16) of Part I if

$$(1 - C) \geq 0. \tag{2.43}$$

Alternatively, the modified equation is another way to obtain this. The first (even) term on the right hand of Eq. (2.28), which acts as a diffusion term, must always be positive for T_j^n not to be inflamed in time; i.e. has to satisfy Eq. (2.43), implying that the Courant-Isaacson-Rees scheme is indeed conditionally stable.

2.5.4. **Accuracy.** We thirdly investigate how accurate, both in magnitude and in phase, the numerical solution is using the Hirt's and von Neumann's complementary analysis.

On the one hand, by applying the discrete Fourier series grid solution of Eq. (2.1) of Part I to the Courant-Isaacson-Rees modified equation (2.40) truncated up to the four-order derivatives we see that the damping term of the numerical solution is not unity as it should be but it is given by

$$\exp\left[- \left(\frac{C - C^2}{2} \right) \frac{(\Delta x)^2}{\Delta t}\, k^2\, \Delta t \right], \tag{2.44}$$

which is shown in left panel of Fig. 11.

Alternatively, since the exact growth factor is equal to unity, the relative amplitude error (Eq. (2.29) of Part I) is given by

$$\delta A = \sqrt{1 - 2C(1 - C)[1 - \cos(k\Delta x)]} - 1. \tag{2.45}$$

and is shown in right panel of Fig. 11 where we find, in agreement with the left panel, that it increases outside the stability region, is 0 for $C = 1$,

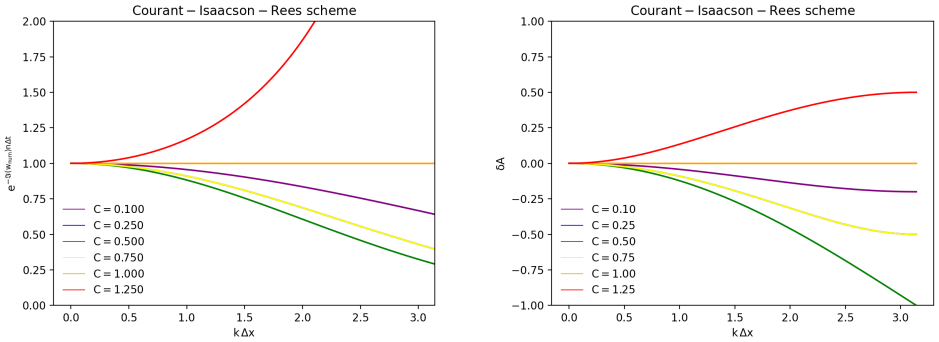

FIGURE 11. Damping factor (approximated to the four-order derivatives) and relative amplitude error as a function of phase angle or frequency, in radians, for specific C number values.

and decreases rapidly from 0 at $k\Delta x = 0$ (for consistency reasons) when the frequency increases (the yellow line and the blue one are the same line). We shall point out later that this dissipative rapid decrease is typically seen in first order schemes. We also find that the strongest damping occurs at $C = 0.5$ because this value maximizes $2C(1 - C)$, which will be relevant to the kinetic regimes that follow.

On the other hand, by applying the discrete Fourier series grid solution of Eq. (2.1) of Part I to the Courant-Isaacson-Rees modified equation (2.28) truncated up to the five-order derivatives, then we see that the dispersive term is given by

$$\exp\left\{i\,k\,\left[x - v\,t + \frac{1}{6}(C - 3\,C^2 + 2\,C^3)\frac{(\Delta x)^3}{\Delta t}\,k^2\,t\right]\right\}, \tag{2.46}$$

implying the dispersive phase velocity shown in Fig. 12. Surprisingly, here we find that the instantaneous velocity flips sign twice (the green line and the orange one are the same line), when $C = 0.5$, and when $C = 1$ (the blue line and the red one are the same line). For $C < 0.5$ we find a numerical propagation speed smaller than the physical one, but shifting closer to the physical one with increasing C's. This leads to the very striking fact that the instantaneous velocity flips sign once a threshold is reached, when the numerical speed reaches exact value at $C = 0.5$, but while the damping is strong enough to prevent unstable numerical growth. Then for $C > 0.5$ the trend reverses and hence a new cycle begins having a numerical propagation speed larger than the

physical one, but shifting again closer to the physical one with increasing C's. Again this leads to that the instantaneous velocity flips sign once the same threshold is again reached, when the numerical speed again reaches exact value at $C = 1$, which is nondamping implying, this second time, instability. More on this later.

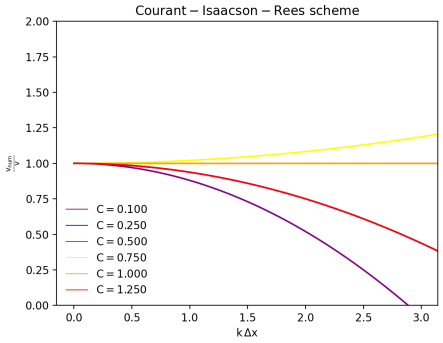

FIGURE 12. The phase velocity of the Courant-Isaacson-Rees solution (approximated to the four-order derivatives), Eq. (2.46) vs. frequency in radians, for specific C values which are distinguished by line colors.

Incidentally, we also can obtain these coefficients of diffusion and dispersion from by differentiating Eq. (2.42) with respect to k; specifically

$$\frac{1}{2}\left.\frac{\partial^2 w_n}{\partial k^2}\right|_{k=0} = \left(\frac{C - C^2}{2}\right)\frac{(\Delta x)^2}{\Delta t}, \tag{2.47}$$

$$-\frac{1}{6}\left.\frac{\partial^3 w_n}{\partial k^3}\right|_{k=0} = -\left(\frac{C - 3\,C^2 + 2\,C^3}{6}\right)\frac{(\Delta x)^3}{\Delta t}. \tag{2.48}$$

Alternatively, from the von Neumann's complementary analysis point of view, the numerical phase component of the Courant-Isaacson-Rees growth factor, Eq. (2.41), is given by

$$\phi = \arctan\left(\frac{\mathfrak{I}(G)}{\mathfrak{R}(G)}\right) = \arctan\left(\frac{-C\sin(k\Delta x)}{1 - C[1 - \cos(k\Delta x)]}\right), \tag{2.49}$$

which we show in the left panel of the Fig. 13.

Therefore, since the exact phase speed is the $-v$, we present in the right panel of the Fig. 13 the numerical relative phase error (see Eq. (2.30) of Part I) of the Courant-Isaacson-Rees scheme plotted against the phase angle for specific C values.

To shed light on the stability issue is key to consider left panel in Fig. 13 where we find, in perfect agreement with findings from 12, that for $C < 0.5$ waves have leading shift but shift closer to the $\delta\phi = 0$ (in the right panel in Fig. 13 the green line and the orange one are the same line) up to the stability threshold is reached when we have no dispersion error, the relative phase shift error flips sign and the Fourier modes have just the opposite, i.e. lagging shift. Now only short waves with $C < 0.5$ are poorly resolved, quasi-stationary waves. Nevertheless, for $0.5 < C < 1$ the modes stay in the stable regimen and continue shifting closer to the $\delta\phi = 0$ (see the right panel in Fig. 13) up to the stability threshold is again reached when we have no dispersion error either, the relative phase shift error flips sign again and the Fourier modes have again leading shift but now driving the solution to instability since, unlike the case when $C = 0.5$, with $C = 1$ the diffusion vanishes when we do reach the analytic solution. In fact, we finally deduce that Eq. (2.1) reduces to $T_j^{n+1} = T_{j-1}^n$ if $C = 1$, the exact solution (see A). The same as the Richardson's scheme but in a direct way. In other words, its only error comes from the discretization of the initial condition. However, this does not happen in general; i.e. does not necessarily hold in nonlinearities.

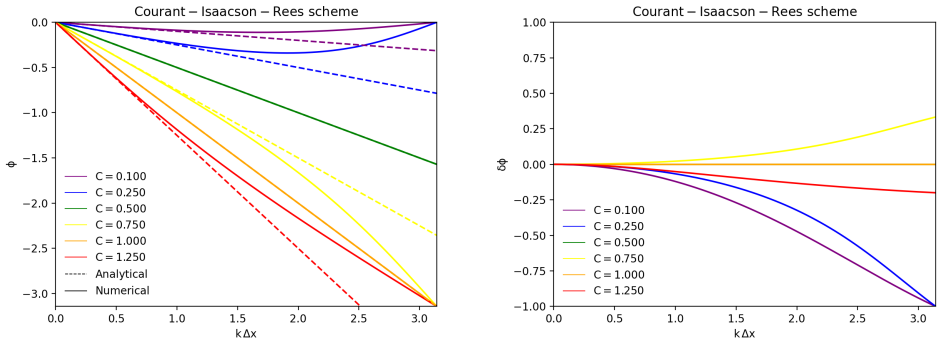

FIGURE 13. Left: the numerical phase component. Right: the numerical relative phase error as a function of phase angle or frequency, in radians, for specific C number values.

2.5.5. **Monotonicity.** Finally, from the Eq. (2.38) the coefficients of the new solution are $1 - C$ and C. That is, they are all positive in the stability region, Eq. (2.43). Hence, this Courant-Isaacson-Rees scheme behaves monotonically.

2.6. **The Lax's 1954 single-step explicit scheme.**

2.6.1. **Construction.** In 1954 Lax [13] presented a scheme that overcomes the stability problem due to the Schmidt's scheme, we found in the Eq. (2.18), in exactly the same way as Du Fort and Frankel evaded the stability problem due to the Richardson's scheme in the case of the heat equation (see Paper I):

$$\frac{T_j^{n+1} - \left(\frac{T_{j-1}^n + T_{j+1}^n}{2}\right)}{\Delta t} = -v\frac{T_{j+1}^n - T_{j-1}^n}{2\Delta x}, \tag{2.50}$$

i.e. by taking the space average of T_j^n at (x_j, t^n).

2.6.2. **Consistency and order of accuracy.** We firstly analyze the consistency of the scheme using the Hirt's method. Substituting each value of T at points other than point (x_j, t^n) in the scheme in a Taylor series around the value T_j^n at that point (x_j, t^n), i.e. we substitute Eqs. 2.6 and 2.13 of Part I in Eq. (2.50), gives

$$\frac{\partial T}{\partial t} + v\frac{\partial T}{\partial x} = \frac{(\Delta x)^2}{2\,\Delta t}\frac{\partial^2 T}{\partial x^2} - \frac{\Delta t}{2}\frac{\partial^2 T}{\partial t^2} - \frac{v\,(\Delta x)^2}{6}\frac{\partial^3 T}{\partial x^3} - \frac{(\Delta t)^2}{6}\frac{\partial^3 T}{\partial t^3} + \cdots . \tag{2.51}$$

We thus see from that equation, which is not yet the modified equation, that the first term on the right hand side goes to infinity when $\Delta t \to 0$ independently of Δx and therefore the Lax's scheme of calculation is inconsistent for any value of $\frac{(\Delta x)^2}{\Delta t}$ (i.e. it converges to that of a parabolic equation). However, if a time step $\Delta t \sim \Delta x$ is used we then achieve first order accuracy. That is, the Lax's scheme is conditionally consistent and we must now to be careful in choosing the time step to assure the consistency of the scheme (if we want to use it, for its other virtues). We should realize the reason for their non consistency is that Lax changed the method after he (really Schmidt) has made the Taylor expansions in the usual way, the same as the Du Fort-Frankel scheme (see Paper I).

We furthermore provide here the evolution equation with only space derivatives, i.e. the modified equation. In order to achieve it, we firstly find expressions for $\frac{\partial^2 T}{\partial t^2}$ and $\frac{\partial^3 T}{\partial t^3}$, and secondly (be careful with this) for $\frac{\partial^2 T}{\partial x \partial t}$, $\frac{\partial^3 T}{\partial x^2 \partial t}$ and $\frac{\partial^3 T}{\partial x \partial t^2}$, by differentiating Eq. (2.51); all of which we use systematically to eliminate the time derivatives in it. This implies that the modified equation associated with the Lax's scheme, the equation of

the grid function from Lax's difference equation, is:

$$\frac{\partial T}{\partial t}+v\frac{\partial T}{\partial x}=\left(\frac{1-C^2}{2}\right)\frac{(\Delta x)^2}{\Delta t}\frac{\partial^2 T}{\partial x^2}+\left(\frac{C-C^3}{3}\right)\frac{(\Delta x)^3}{\Delta t}\frac{\partial^3 T}{\partial x^3} + \left(\frac{4-4\,C^2-6\,C^4}{24}\right)\frac{(\Delta x)^4}{\Delta t}\frac{\partial^4 T}{\partial x^4}+\mathcal{O}((\Delta x)^5), \tag{2.52}$$

which is one of two ways to next not only calculate the local error but also estimate the stability.

2.6.3. **Stability.** We secondly now analyze the stability using the von Neumann's method. Substituting a term of Eq. (2.1) of Part I into each term a term in Eq. (2.50) we get the following complex valued, growth factor associated with the Lax's scheme:

$$G=\frac{1}{2}(e^{i\,k\,\Delta x}+e^{-i\,k\,\Delta x})-\frac{1}{2}C(e^{i\,k\,\Delta x}+e^{-i\,k\,\Delta x})=\cos{(k\Delta x)}-i\,C\sin{(k\Delta x)}, \tag{2.53}$$

whose magnitude component takes the form

$$|G|^2=\cos^2{(k\Delta x)}+C^2\sin^2{(k\Delta x)}, \tag{2.54}$$

which since $\cos^2{(k\Delta x)}\leq 1$ and $\sin^2{(k\Delta x)}\leq 1$, satisfies Eq. (2.16) of Part I if

$$(1-C)\geq 0. \tag{2.55}$$

Alternatively, the modified equation is another way to obtain this. The first (even) term on the right hand of Eq. (2.28), which acts as a diffusion term, must always be positive for T_j^n not to be inflamed in time; i.e. has to satisfy Eq. (2.55), implying that the Lax's scheme is indeed conditionally stable.

2.6.4. **Accuracy.** We thirdly investigate how accurate, both in magnitude and in phase, the numerical solution is using the Hirt's and von Neumann's complementary analysis.

On the one hand, by applying the discrete Fourier series grid solution of Eq. (2.1) of Part I to the Lax's modified equation (2.52) through fifth order we see that the damping term of the numerical solution is not unity as it should be but it is given by

$$\exp\left[-\left(\frac{1-C^2}{2}\right)\frac{(\Delta x)^2}{\Delta t}k^2\,\Delta t+\left(\frac{4-4\,C^2-6\,C^4}{24}\right)\frac{(\Delta x)^4}{\Delta t}\,k^4\,\Delta t\right], \tag{2.56}$$

which is shown in left panel of Fig. 14.

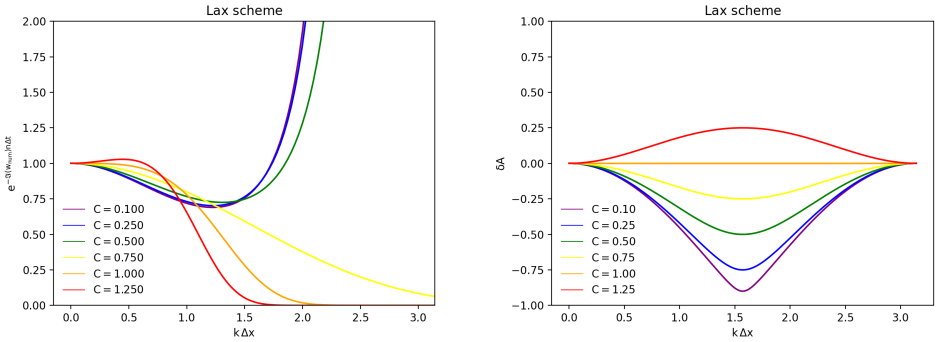

FIGURE 14. Damping factor (approximated to the five-order derivatives) and relative amplitude error as a function of phase angle or frequency, in radians, for specific C number values.

Alternatively, since the exact growth factor is equal to unity, the relative amplitude error (Eq. (2.29) of Part I) is given by

$$\delta A = \sqrt{\cos^2(k\Delta x) + C^2 \sin^2(k\Delta x)} - 1, \tag{2.57}$$

and is shown in right panel of Fig. 14 where we find, in agreement with the left panel remembering this is obtaining by truncating the numerical solution up to the five-order derivatives, that it increases outside the stability region, is 0 for $C = 1$, and both decreases rapidly (typical for first order schemes) from 0 at $k\Delta x = 0$ (for consistency reasons) to $C - 1$ (see Eq. (2.57)) at $k\Delta x = \pi/2$ and increases to 0 again at $k\Delta x = \pi$, i.e. the Lax's scheme has no diffusion error for the highest frequency. The same as the Laasonen's scheme, although its effect is much greater than that of the Laasonen's scheme. Up to now, it is furthermore worth emphasizing that this error takes its maximum value for the approximately uniformly dissipative Courant-Isaacson-Rees scheme.

On the other hand, by applying the discrete Fourier series grid solution of Eq. (2.1) of Part I to the Lax's modified equation (2.28) truncated up to the five-order derivatives, then we see that the dispersive term is given by

$$\exp\left\{i\,k\,\left[x - v\,t - \left(\frac{1 - C^2}{3}\right)\frac{(\Delta x)^3}{\Delta t}\,k^2\,t\right]\right\}, \tag{2.58}$$

implying the dispersive phase velocity shown in Fig. 15. We now find a numerical propagation speed higher than the physical one, but shifting

closer to the physical one with increasing C's. This leads to the striking fact that the instantaneous velocity flips sign once a stability-threshold is reached, when the numerical speed reaches exact value. The same as the Richardson's scheme, although in backwards. More on this later.

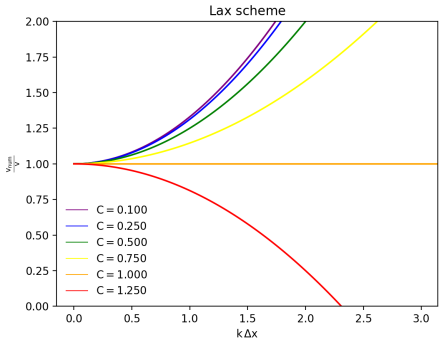

FIGURE 15. The phase velocity of the Lax's solution (approximated to the five-order derivatives), Eq. (2.58) vs. frequency in radians, for specific C values which are distinguished by line colors.

Alternatively, from the von Neumann's complementary analysis point of view, the numerical phase component of the Lax's growth factor, Eq. (2.53), is given by

$$\phi = \arctan\left(\frac{\Im(G)}{\Re(G)}\right) = \arctan\left(-C\tan\left(k\Delta x\right)\right), \tag{2.59}$$

which we show in the left panel of the Fig. 16.

Therefore, since the exact phase speed is the $-v$, we present in the right panel of the Fig. 16 the numerical relative phase error (see Eq. (2.30) of Part I) of the Lax's scheme plotted against the phase angle for specific C values.

To shed more light on the stability issue is again key to consider left panel in Fig. 16. On one hand, as opposed to the surprising short waves, concerning the long waves we observe that they reproduce the behavior typically observed in Fig. 15. For $C < 1$ waves have lagging shift, everywhere $\delta\phi > 0$, showing that the numerical solution leads the physical solution; but shift closer to the $\delta\phi = 0$, once the stability threshold is reached, when the relative phase shift error flips sign and the Fourier modes will have leading shift. In other words, the (long)

waves reach the physical speed independently of the grid velocity $\frac{\Delta x}{\Delta t}$; however, the greater the grid velocity, the greater the variation it has to undergo to equal the physical velocity and so the greater the spurious bias we observe in the right panel in Fig. 16. On the other hand, the nonintuitive opposing behavior we find concerning the still stable short waves is consistent with the mentioned consistency restriction because for these waves Δt has to be much too small for consistency, which leads to the low accuracy observed in the right panel in Fig. 16 vs. Eq. (2.59); that is to say, the smaller the C value, the faster propagation speed and the poorer accuracy as showed in the rigth panel in Fig. 16, that is to say, the short waves are incorrectly propagated.

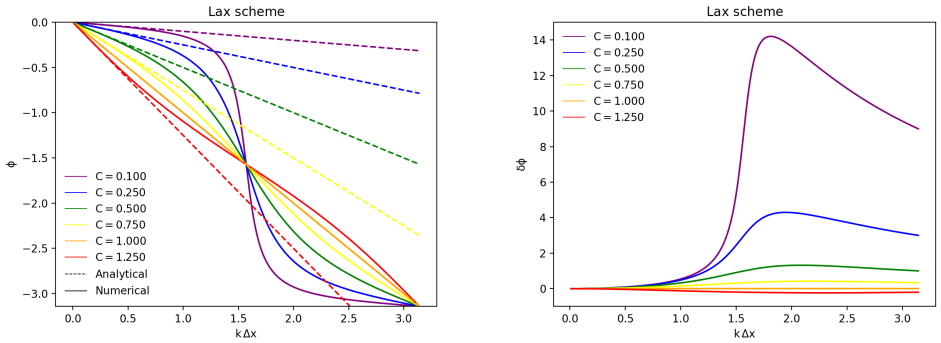

FIGURE 16. Left: the numerical phase component. Right: the numerical relative phase error as a function of phase angle or frequency, in radians, for specific C number values.

Finally, we also deduce that Eq. (2.50) reduces to $T_j^{n+1} = T_{j-1}^n$ if $C = 1$, the exact solution (see A), as we can also see in Fig. 16. The same as the Courant-Isaacson-Rees scheme. However, any other C suffers a poor, even-odd decoupling because T_j^{n+1} only depends on T_{j+1}^n and T_{j-1}^n which is clearly visible in Table 1. The same as the Richardson's scheme.

2.6.5. **Monotonicity.** Finally, from the Eq. (2.38) the coefficients of the new solution are $\frac{1}{2}(1-C)$ and $\frac{1}{2}(1-C)$. That is, they are all positive in the stability region. Hence, this Lax's scheme is monotone.

2.7. **The Lax-Richtmyer 1956 single-step semi-explicit scheme.**

2.7.1. **Construction.** In 1956 Lax and Richtmyer [14] considered the same discretization as Lax did, but evaluating the space derivative forwards in time; i.e.,

$$\frac{T_j^{n+1} - \left(\frac{T_{j-1}^n + T_{j+1}^n}{2}\right)}{\Delta t} = -v\frac{T_{j+1}^{n+1} - T_{j-1}^{n+1}}{2\Delta x}. \tag{2.60}$$

Hence this scheme is not based on Taylor series expansions, either.

Table 1 emphasizes that Eq. (2.60) is time-implicit. The same as the Crank-Nicolson scheme.

2.7.2. **Consistency and order of accuracy.** We firstly analyze the consistency of the scheme using the Hirt's method. Substituting each value of T at points other than point (x_j, t^{n+1}) in the scheme in a Taylor series around the value T_j^{n+1} at that point (x_j, t^{n+1}), i.e. we substitute Eqs. 2.6, 2.12 and 2.13 of Part I in Eq. (2.26), gives

$$\frac{\partial T}{\partial t} + v\frac{\partial T}{\partial x} = \frac{\Delta t}{2}\frac{\partial^2 T}{\partial t^2} - \frac{v\,(\Delta x)^2}{6}\frac{\partial^3 T}{\partial x^3} - \frac{(\Delta t)^2}{6}\frac{\partial^3 T}{\partial t^3} + \cdots . \tag{2.61}$$

We then see from that equation, which is not yet the modified equation, that the right hand side vanishes when $\Delta t \to 0$ and $\Delta x \to 0$ and therefore the Lax-Richtmyer scheme of calculation is consistent. In addition, this side goes to zero as the first power of Δt and the second power of Δx, implying that the scheme is of first order accuracy in time and second order accuracy in space as well.

We furthermore provide here the evolution equation with only space derivatives, i.e. the modified equation. In order to achieve it, we firstly find expressions for $\frac{\partial^2 T}{\partial t^2}$ and $\frac{\partial^3 T}{\partial t^3}$, and secondly (be careful with this) for $\frac{\partial^3 T}{\partial t^3}$, $\frac{\partial^2 T}{\partial x \partial t}$ and $\frac{\partial^3 T}{\partial x^2 \partial t}$, by differentiating Eq. (2.61); all of which we use systematically to eliminate the time derivatives in it. This implies that the modified equation associated with the Lax-Richtmyer scheme, the equation of the grid function from Lax-Richtmyer difference equation, is:

$$\begin{aligned}\frac{\partial T}{\partial t} + v\frac{\partial T}{\partial x} = &\left(\frac{1 + C^2}{2}\right)\frac{(\Delta x)^2}{\Delta t}\frac{\partial^2 T}{\partial x^2} - \left(\frac{C + 2\,C^3}{6}\right)\frac{(\Delta x)^3}{\Delta t}\frac{\partial^3 T}{\partial x^3} \\ &+ \left(\frac{-2 + 6\,C^2}{24}\right)\frac{(\Delta x)^4}{\Delta t}\frac{\partial^4 T}{\partial x^4} + \mathcal{O}((\Delta x)^5),\end{aligned} \tag{2.62}$$

which is one of two ways to next not only calculate the local error but also estimate the stability.

2.7.3. **Stability.** We secondly now analyze the stability using the von Neumann's method. Substituting a term of Eq. (2.1) of Part I into each term a term in Eq. (2.60) we get the following complex valued, growth factor associated with the Lax-Richtmyer scheme:

$$G = \frac{\cos(k\Delta x)}{1 + i\,C\sin(k\Delta x)}, \tag{2.63}$$

whose magnitude component takes the form

$$|G| = \sqrt{\frac{\cos^2(k\Delta x)}{1 + C^2\sin^2(k\Delta x)}} < 1, \tag{2.64}$$

which satisfies Eq. (2.16) of Part I and thus the Lax-Richtmyer scheme is stable for the advection equation.

Alternatively, the modified equation is another way to obtain this. The first (even) term on the right hand of Eq. (2.28), which acts as a diffusion term, always is positive implying that the Lax-Richtmyer scheme is indeed unconditionally stable.

In fact, this property of being stable turns out to be true for all purely implicit schemes. That said, if not for stability, for accuracy we cannot use a large time step. To clearly see it, note the ratio of the Lax-Richtmyer numerical damping rate (from Eq. (2.28) of Part I, $e^{-iw_{num}\Delta t} = |G|$) to the exact damping rate (the unity) is

$$\frac{w_{num}}{w} = \ln\left(\frac{\cos(k\Delta x)}{\sqrt{1 + C^2\sin^2(k\Delta x)}}\right) = \frac{1}{2}\left(-1 - C^2\right)(k\Delta x)^2 + \mathcal{O}((k\Delta x)^4); \tag{2.65}$$

which show us that for, e.g., $C = 0.5$ the error on the damping rate is as much as about the exact damping rate (Eq. (2.65) is on average about 1).

2.7.4. **Accuracy.** We thirdly investigate how accurate, both in magnitude and in phase, the numerical solution is using the Hirt's and von Neumann's complementary analysis.

On the one hand, by applying the discrete Fourier series grid solution of Eq. (2.1) of Part I to the Lax-Richtmyer modified equation (2.28) truncated up to the five-order derivatives we see that the damping term of the numerical solution is not unity as it should be but it is given by

$$\exp\left(\left[-\left(\frac{1 + C^2}{2}\right)\frac{(\Delta x)^2}{\Delta t}k^2\,\Delta t + \left(\frac{-2 + 6\,C^2}{24}\right)\frac{(\Delta x)^4}{\Delta t}k^4\,\Delta t\right]\right), \tag{2.66}$$

which is shown in left panel of Fig. 17.

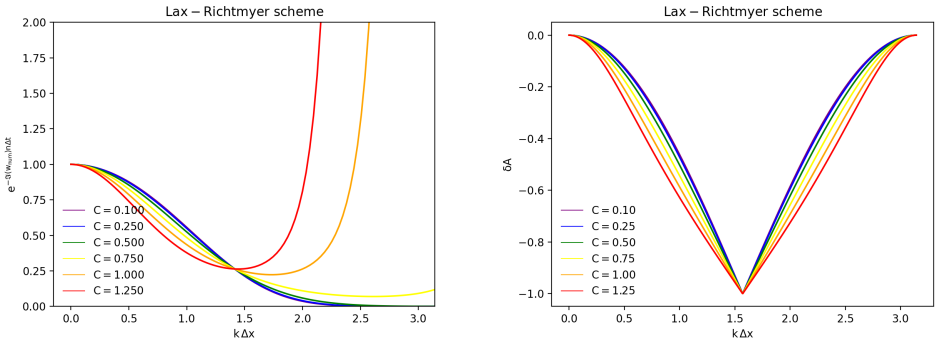

FIGURE 17. Damping factor (approximated to the five-order derivatives) and relative amplitude error as a function of phase angle or frequency, in radians, for specific C number values.

Alternatively, since the exact growth factor is equal to unity, the relative amplitude error (Eq. (2.29) of Part I) is given by

$$\delta A = \sqrt{\frac{\cos^2(k\Delta x)}{1 + C^2 \sin^2(k\Delta x)}} - 1, \tag{2.67}$$

and is shown in right panel of Fig. 17 where we find, in agreement with the left panel remembering this is obtaining by truncating the numerical solution up to the five-order derivatives, that it both decreases rapidly (typical for first order schemes) from 0 at $k\Delta x = 0$ (for consistency reasons) to -1 (see Eq. (2.67)) at $k\Delta x = \pi/2$ and increases rapidly to 0 again at $k\Delta x = \pi$; i.e. the Lax-Richtmyer scheme is not uniformly dissipative. It has no diffusion error for the highest frequency. The same as the Lax's scheme but much worse.

On the other hand, by applying the discrete Fourier series grid solution of Eq. (2.1) of Part I to the Lax-Richtmyer modified equation (2.62) truncated up to the five-order derivatives, then we see that the dispersive term is given by

$$\exp\left\{i\,k\,\left[x - v\,t + \frac{1}{6}(C + 2\,C^3)\frac{(\Delta x)^3}{\Delta t}\,k^2\,t\right]\right\}, \tag{2.68}$$

implying the dispersive phase velocity shown in Fig. 18. We find a numerical propagation speed smaller than the physical one, but moving

away from the physical one with increasing C's. This leads to the fact that the instantaneous velocity does not flip sign because the numerical speed never reaches exact value, implying the Lax-Richtmyer scheme don't have instability issue. More on this later.

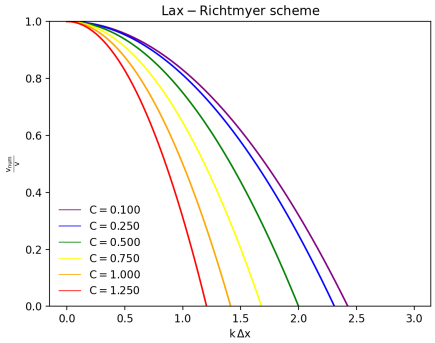

FIGURE 18. The phase velocity of the Lax-Richtmyer solution (approximated to the five-order derivatives), Eq. (2.68) vs. frequency in radians, for specific C values which are distinguished by line colors.

Alternatively, from the von Neumann's complementary analysis point of view, the numerical phase component of the Lax-Richtmyer growth factor, Eq. (2.63), is given by

$$\phi = \arctan\left(\frac{\Im(G)}{\Re(G)}\right) = \arctan\left[-C\sin\left(k\Delta x\right)\right], \tag{2.69}$$

the same as the Laasonen's scheme which we show in the left panel of the Fig. 19.

Therefore, since the exact phase speed is the $-v$, we present in the right panel of the Fig. 19 the numerical relative phase error (see Eq. (2.30) of Part I) of the Lax-Richtmyer scheme plotted against the phase angle for specific C values.

We find that the (dispersive) behavior is identical to that of the Laasonen's scheme and similar to that using the Crank-Nicolson scheme. Indeed, the left panel of Fig. 19 shows us that for all values of C we have leading shift, the relative phase error is less than 0, indicating a numerical propagation speed smaller than the physical one; but shift away from the line $\delta\phi = 0$ (see the left panel of Fig. 19), implying again the Lax-Richtmyer scheme don't have instability issue, either. However, let's

not forget that the dissipative behavior is much worse than that using both the Laasonen's and the Crank-Nicolson schemes.

2.7.5. **Monotonicity.** Although the Lax-Richtmyer scheme is semi-implicit the convex combination technique still fails to estimate its monotonicity because T_j^{n+1} depends on space average of T_j^n, i.e. in practice it depends only on T_j^n. Therefore we must demonstrate Eq. (2.31) of Part I from Eq. (2.60) (see Table 1); which is, indeed, exactly the same as we did for the Laasonen's scheme. Hence, the Lax-Richtmyer scheme is monotone and does not introduce oscillations.

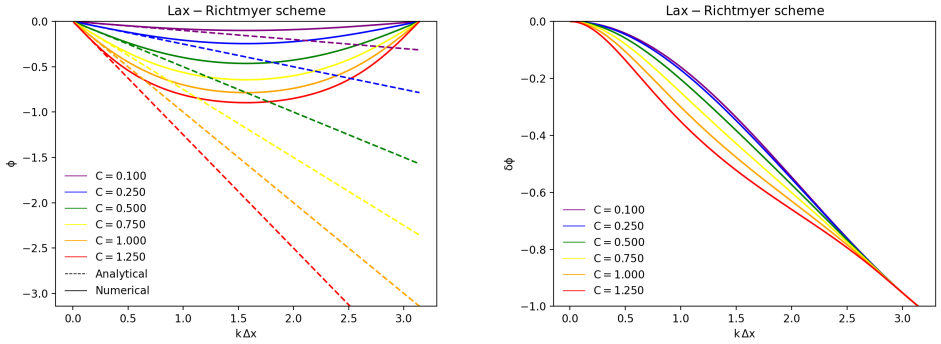

FIGURE 19. Left: the numerical phase component. Right: the numerical relative phase error as a function of phase angle or frequency, in radians, for specific C number values.

2.8. The Wendroff's 1958 single-step semi-explicit scheme.

2.8.1. **Construction.** In 1958 Wendroff [15] was the first to come up with an alternative to the Crank-Nicolson scheme by averaging between n and n+1 time levels the following semi-discretized, forward approximation (to advection equation)

$$\frac{1}{2}\left(\frac{\partial T_j}{\partial t}+\frac{\partial T_{j-1}}{\partial t}\right)=-v\left(\frac{T_j-T_{j-1}}{\Delta x}\right), \tag{2.70}$$

to obtain the following compact scheme:

$$\frac{1}{2}\left(\frac{T_j^{n+1}-T_j^n}{\Delta t}+\frac{T_{j-1}^{n+1}-T_{j-1}^n}{\Delta t}\right)=-v\,\frac{1}{2}\left(\frac{T_j^{n+1}-T_{j-1}^{n+1}}{\Delta x}+\frac{T_j^n-T_{j-1}^n}{\Delta x}\right). \tag{2.71}$$

Hence this scheme is not based on Taylor series expansions, either.

Table 1 emphasizes that Eq. (2.71) is time-implicit. The same as the Crank-Nicolson scheme.

2.8.2. **Consistency and order of accuracy.** We firstly analyze the consistency of the scheme using the Hirt's method. The same as the Crank-Nicolson scheme, we must reduce the number of indexes in it before raising and/or lowering them. Thus, in this situation we rewrite Eq. (2.71) as $T^{n+1}_{j-1/2} - T^{n}_{j-1/2} + C\,T^{n+1/2}_{j} - C\,T^{n+1/2}_{j-1} = 0$. Next, substituting each value of T at points other than point $(x_{j-1/2}, t^{n+1/2})$ in this equation in a Taylor series around the value T^n_j at that point $(x_{j-1/2}, t^{n+1/2})$, gives

$$\frac{\partial T}{\partial t} + v\frac{\partial T}{\partial x} = -\frac{C\,(\Delta x)^3}{24\,\Delta t}\frac{\partial^3 T}{\partial x^3} - \frac{(\Delta t)^2}{24}\frac{\partial^3 T}{\partial t^3} + \cdots . \tag{2.72}$$

We then see from that equation, which is not yet the modified equation, that the right hand side vanishes when $\Delta t \to 0$ and $\Delta x \to 0$ and therefore the Wendroff's scheme of calculation is consistent. In addition, this side goes to zero as the second power of Δt and the second power of Δx, implying that the scheme is of second order accuracy in both time and space.

We furthermore provide here the evolution equation with only space derivatives, i.e. the modified equation. In order to achieve it, we firstly find expressions for $\frac{\partial^3 T}{\partial t^3}$, and secondly (be careful with this) for $\frac{\partial^3 T}{\partial x^2 \partial t}$, by differentiating Eq. (2.72); all of which we use systematically to eliminate the time derivatives in it. This implies that the modified equation associated with the Wendroff's scheme, the equation of the grid function from Wendroff's difference equation, is:

$$\frac{\partial T}{\partial t} + v\frac{\partial T}{\partial x} = \left(\frac{C^3 - C}{24}\right)\frac{(\Delta x)^3}{\Delta t}\frac{\partial^3 T}{\partial x^3} + \mathcal{O}((\Delta x)^4), \tag{2.73}$$

which is one of two ways to next not only calculate the local error but also estimate the stability.

2.8.3. **Stability.** We secondly now analyze the stability using the von Neumann's method. Substituting a term of Eq. (2.1) of Part I into each term a term in Eq. (2.71) we get the following complex valued, growth factor associated with the Wendroff's scheme:

$$G = \frac{1 - C + (1 + C)\,e^{(-i\,k\,\Delta x)}}{1 + C + (1 - C)\,e^{(-i\,k\,\Delta x)}} = 1, \tag{2.74}$$

i.e. the amplitudes of the Fourier components neither increases nor decrease as time evolves, which is a desirable property because is in line

with the lack of diffusion of the general analytical solution (Eq. (2.18) of Part I). Hence, the Wendroff's scheme is stable even at large time step size, although (be careful with this) this will not necessarily give accurate solution. This is because, the non-explicit schemes use the information from neighboring cell of the current time step to find the solution. The same as the Crank-Nicolson scheme.

Alternatively, the Hirt's method is another way to obtain this. The first term on the right hand of Eq. (2.73) is odd (which acts as a dispersive term) and there is no even-order derivatives, as we have just obtained. That way, Wendroff's scheme is stable, neutrally stable. The same as the Crank-Nicolson scheme.

2.8.4. **Accuracy.** We thirdly investigate how accurate, both in magnitude and in phase, the numerical solution is using the Hirt's and von Neumann's complementary analysis.

On the one hand, by applying the discrete Fourier series grid solution of Eq. (2.1) of Part I to the Wendroff's modified equation (2.73) we see that there is only odd-order derivatives, implying the damping term of the numerical solution is clearly unity (see Eq. (2.27) of Part I) which is shown in left panel of Fig. 20.

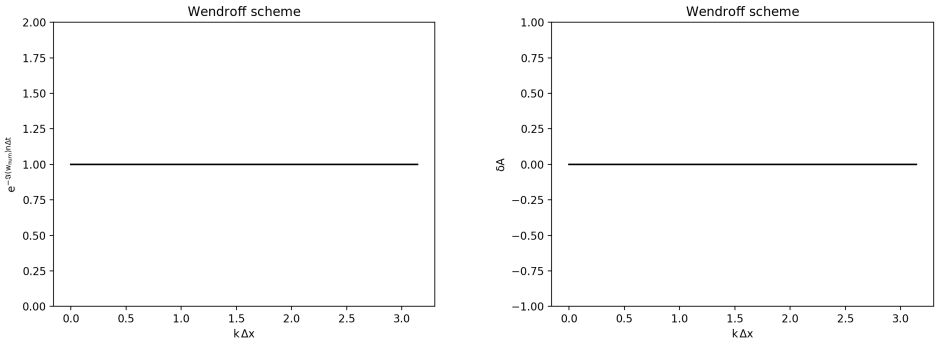

FIGURE 20. Damping factor and relative amplitude error as a function of phase angle or frequency, in radians, for specific C number values.

Alternatively, since the exact growth factor is equal to unity, the relative amplitude error (Eq. (2.29) of Part I) is given by

$$\delta A = 0, \tag{2.75}$$

as shown in right panel of Fig. 20. The same as the Richardson's scheme.

On the other hand, by applying the discrete Fourier series grid solution of Eq. (2.1) of Part I to the Wendroff's modified equation (2.73) truncated up to the five-order derivatives, then we see that the dispersive term is given by

$$\exp\left\{i\,k\,\left[x - v\,t + \left(\frac{C^3 - C}{24}\right)\frac{(\Delta x)^3}{\Delta t}\,k^2\,t\right]\right\}, \tag{2.76}$$

implying the dispersive phase velocity shown in Fig. 21. We now find a numerical propagation speed higher than the physical one, but decelerating and shifting closer to the physical one with increasing C's. This leads to the striking fact that the instantaneous velocity flips sign when the numerical speed reaches exact value, while stays stable (Eq. (2.74)). This effect is the same as that in the Lax's scheme but much smaller, however staying stable even if the instantaneous velocity changes sign. More on this later.

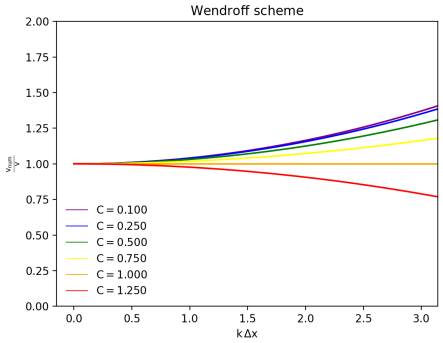

FIGURE 21. The phase velocity of the Wendroff's solution (approximated to the four-order derivatives), Eq. (2.76) vs. frequency in radians, for specific C values which are distinguished by line colors.

Equivalently, from the von Neumann's complementary analysis point of view, the numerical phase component of the Wendroff's growth factor, Eq. (2.74), is given by

$$\phi = \arctan\left(\frac{\Im(G)}{\Re(G)}\right) = \arctan\left[\frac{-2\,C\,\tan\left(\frac{k\Delta x}{2}\right)}{1 - C^2\,\tan^2\left(\frac{k\Delta x}{2}\right)}\right], \tag{2.77}$$

which we show in the left panel of the Fig. 22.

Therefore, since the exact phase speed is the $-v$, we present in the right panel of the Fig. 22 the numerical relative phase error (see Eq. (2.30) of Part I) of the Wendroff's scheme plotted against the phase angle for specific C values.

To shed even more light on the stability issue is key to consider left panel in Fig. 22 where we find, in perfect agreement with findings from 21, that for $C < 1$ the waves have lagging shift, everywhere $\delta\phi > 0$ (see the left panel of Fig. 22), showing that the numerical solution leads the physical solution; but shift closer to the line $\delta\phi = 0$, once the physical solution is reached for $C = 1$, when the relative phase shift error flips sign and the Fourier modes will have leading shift. In other words, the fast waves decelerate and reach the physical speed independently of the grid velocity $\frac{\Delta x}{\Delta t}$; however, the greater the grid velocity, the greater the variation it has to undergo to equal the physical velocity and so the greater the spurious bias with the fast high frequency waves we observe in the right panel in Fig. 22, that is to say, the shorter wave length, the faster propagation speed, and faster still the smaller the C value. Now, however, the Fourier harmonics do not drive the solution to instability since, unlike either the Richardson's or Lax's cases, the Wendroff's scheme is nonexplicit which is dissipative in nature. In fact, the Wendroff's scheme, unlike the Richardson's scheme, has no computational mode; and, unlike Lax's scheme, is neutrally stable. Hence, let us say that the Wendroff's scheme is not only neutrally but marginally stable.

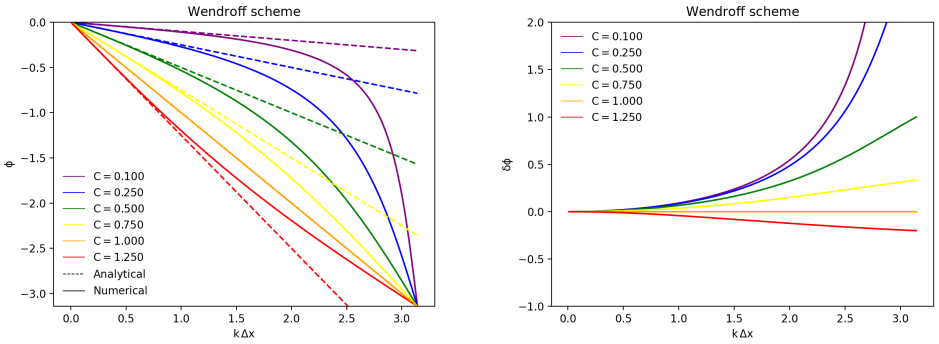

FIGURE 22. Left: the numerical phase component. Right: the numerical relative phase error as a function of phase angle or frequency, in radians, for specific C number values.

Finally, we also deduce that Eq. (2.71) reduces to $T_j^{n+1} = T_{j-1}^n$ if $C = 1$, the exact solution (see A); as we can also see in Fig. 22. Indeed, for $C = 1$ we have no dispersion error (see Fig. 22). The same as the Courant-Isaacson-Rees scheme.

2.8.5. **Monotonicity.** Finally, from the Eq. (2.38) the coefficients of the new solution are $1 - C$ and $1 + C$. That is, they are all positive if $1 - C \geq 0$; which only happens in the non-marginal stability region mentioned earlier. Hence, the Wendroff's scheme is nonmonotone.

2.9. **The Lax-Wendroff 1960 single-step explicit algorithm.**

2.9.1. **Construction.** In 1960 Lax and Wendroff [16] looked for a (second order) accurate scheme but not by introducing additional terms that compensated for the bias caused by the second order spatial discretizations, as both Richardson and especially Crank and Nicolson did, but in a general way. Their derivation rests on the Taylor series expansion (up to the second-order derivatives) of the numerical solution T_i^{n+1} around the node (x_i, t^n), Eq. (2.6) of Part I, and the replacement of its time derivatives by space derivatives by using both the linear (for now this is the way it is in this Part II), differential equation we wish to solve and its derivative,

$$\frac{\partial^2 T}{\partial t^2} = v^2 \frac{\partial^2 T}{\partial x^2}, \tag{2.78}$$

so that they invented:

$$T_j^{n+1} = T_j^n - \Delta t\, v \frac{T_{j+1}^n - T_{j-1}^n}{2\Delta x} + \frac{1}{2}(\Delta t)^2\, v^2 \frac{T_{j-1}^n - 2T_j^n + T_{j+1}^n}{(\Delta x)^2}. \tag{2.79}$$

which is the explicit scheme reformulated in Table 1 using Eq. (2.2) and which however is also based on Taylor series expansions.

2.9.2. **Consistency and order of accuracy.** We firstly analyze the consistency of the scheme using the Hirt's method. Substituting each value of T at points other than point (x_j, t^n) in the scheme in a Taylor series around the value T_j^n at that point (x_j, t^n), i.e. we substitute Eqs. 2.6 and 2.13 of Part I in Eq. (2.79), gives

$$\frac{\partial T}{\partial t} + v\frac{\partial T}{\partial x} = -\frac{v\,(\Delta x)^2}{6}\frac{\partial^3 T}{\partial x^3} - \frac{(\Delta t)^2}{6}\frac{\partial^3 T}{\partial t^3} + \cdots. \tag{2.80}$$

We then see from that equation, which is not yet the modified equation, that the right hand side vanishes when $\Delta t \to 0$ and $\Delta x \to 0$ and therefore the Lax-Wendroff scheme of calculation is consistent. In addition, this

side goes to zero as the second power of Δt and the second power of Δx, implying that the scheme is of second order accuracy in both time and space, as expected by construction.

We furthermore provide here the evolution equation with only space derivatives, i.e. the modified equation. In order to achieve it, we firstly find expressions for $\frac{\partial^3 T}{\partial t^3}$, and secondly (be careful with this) for $\frac{\partial^3 T}{\partial t^3}$ and $\frac{\partial^3 T}{\partial x \partial t^2}$, by differentiating Eq. (2.80); all of which we use systematically to eliminate the time derivatives in it. This implies that the modified equation associated with the Lax-Wendroff scheme, the equation of the grid function from Lax-Wendroff difference equation, is:

$$\frac{\partial T}{\partial t} + v\frac{\partial T}{\partial x} = \left(\frac{C^3 - C}{6}\right)\frac{(\Delta x)^3}{\Delta t}\frac{\partial^3 T}{\partial x^3} + \left(\frac{-C^2 + C^4}{8}\right)\frac{(\Delta x)^4}{\Delta t}\frac{\partial^4 T}{\partial x^4} + \left(\frac{-C - 5\,C^3 + 6\,C^5}{120}\right)\frac{(\Delta x)^5}{\Delta t}\frac{\partial^5 T}{\partial x^5} + \mathcal{O}((\Delta x)^5), \tag{2.81}$$

which is one of two ways to next not only calculate the local error but also estimate the stability.

2.9.3. **Stability.** We secondly now analyze the stability using the von Neumann's method. Substituting a term of Eq. (2.1) of Part I into each term a term in Eq. (2.79) we get the following complex valued, growth factor associated with the Lax-Wendroff scheme:

$$G = 1 - C^2[1 - \cos(k\Delta x)] - i\,C\sin(k\Delta x), \tag{2.82}$$

whose magnitude component takes the form

$$|G|^2 = 1 - C^2(1 - C^2)[1 - \cos(k\Delta x)]^2, \tag{2.83}$$

which satisfies Eq. (2.16) of Part I if

$$(1 - C) \geq 0. \tag{2.84}$$

Alternatively, the modified equation is another way to obtain this. The first term on the right hand of Eq. (2.81), the next-leading-order contribution, is odd which acts as a dispersive term (there is no second-order dissipative derivatives), has to be positive for T_j^n not to be propagated in the opposite direction; i.e. has to satisfy Eq. (2.84). That way, the Lax-Wendroff scheme is conditionally stable. Equivalently, the fourth-order dissipative term must always be positive for T_j^n not to be inflamed in time; i.e. has to satisfy Eq. (2.84), implying that the Lax-Wendroff scheme is indeed conditionally stable.

2.9.4. **Accuracy.** We thirdly investigate how accurate, both in magnitude and in phase, the numerical solution is using the Hirt's and von Neumann's complementary analysis.

On the one hand, by applying the discrete Fourier series grid solution of Eq. (2.1) of Part I to the Lax-Wendroff modified equation (2.81) truncated up to the five-order derivatives we see that the damping term of the numerical solution, which is one order of magnitude smaller than its dispersion, is not unity as it should be but it is given by

$$\exp\left[\left(\frac{-C^2+C^4}{8}\right)\frac{(\Delta x)^4}{\Delta t}\,k^4\,\Delta t\right]. \tag{2.85}$$

which is shown in left panel of Fig. 23.

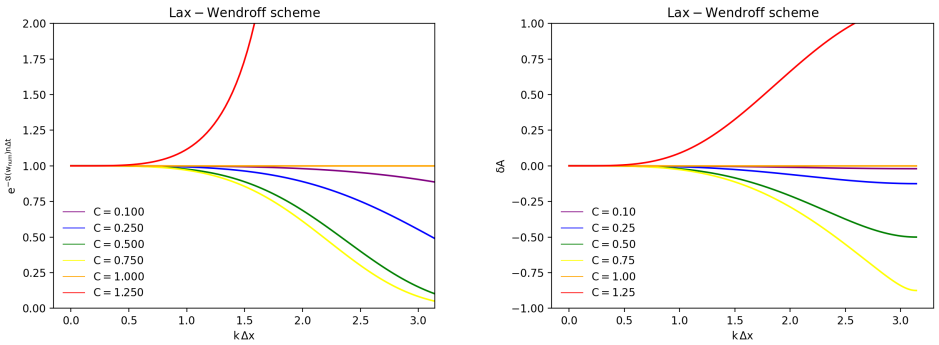

FIGURE 23. Damping factor (approximated to the six-order derivatives) and relative amplitude error as a function of phase angle or frequency, in radians, for specific C number values.

Alternatively, since the exact growth factor is equal to unity, the relative amplitude error (Eq. (2.29) of Part I) is given by

$$\delta A = \sqrt{1 - C^2(1-C^2)[1-\cos(k\Delta x)]^2} - 1, \tag{2.86}$$

as shown in right panel of Fig. 23. The Fig. 23 shows that it increases outside the stability region, is 0 for $C = 1$, and decreases a little from 0 at $k\Delta x = 0$ (for consistency reasons) when the frequency increases. However, we do not expect the rapid decrease typical for first order explicit schemes which found so far with the Courant-Isaacson-Rees scheme but we now observe, as expected from a second order scheme which is this one by Lax and Wendroff, that the region where $\delta A \simeq 0$ is much larger than that found in the Courant-Isaacson-Rees scheme; i.e. the Lax-Wendroff

amplitude error decreases more slowly with increasing frequency than Courant-Isaacson-Rees amplitude error. Also, again, we emphasize that the dissipation error in this Lax-Wendroff scheme is two orders of magnitude smaller than that in a typical scheme with nonzero second order derivative like the Courant-Isaacson-Rees scheme. We also find that the strongest damping occurs at $C = \sqrt{0.5}$ because this value maximizes $C^2(1 - C^2)$, which is relevant to the kinetic regimes that follow.

On the other hand, by applying the discrete Fourier series grid solution of Eq. (2.1) of Part I to the Lax-Wendroff modified equation (2.81) truncated up to the sixth-order derivatives, then we see that the (third order) dispersive term is given by

$$\exp\left\{i\,k\,\left[x - v\,t + \left(\frac{C - C^3}{6}\right)\frac{(\Delta x)^3}{\Delta t}\,k^2\,t\right.\right.$$
$$\left.\left. - \left(\frac{C + 5\,C^3 - 6\,C^4}{120}\right)\frac{(\Delta x)^5}{\Delta t}\,k^4\,t\right]\right\}, \tag{2.87}$$

implying the dispersive phase velocity shown in Fig. 24.

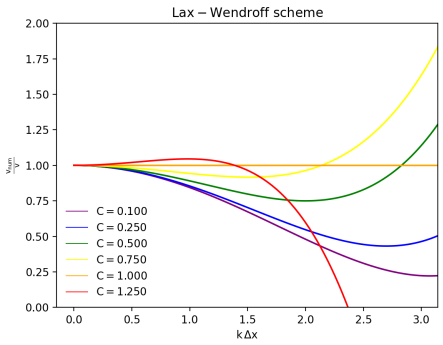

FIGURE 24. The phase velocity of the Lax-Wendroff solution (approximated to the six-order derivatives), Eq. (2.87) vs. frequency in radians, for specific C values which are distinguished by line colors.

Surprisingly enough, in a manner similar to, but not the same as, that which occurs in the Courant-Isaacson-Rees scheme, here we find that the instantaneous velocity flips sign (approximately) twice (remembering this is obtaining by truncating the numerical solution up to the sixth-order derivatives), when $C \simeq 0.5$, in fact when $C = \sqrt{0.5}$, and when $C = 1$. For $C \lesssim 0.5$ we find a numerical propagation speed smaller than

the physical one, but moving closer to the physical one with increasing C's. This leads to the very striking fact that the instantaneous velocity flips sign once a threshold is reached, when the numerical speed reaches exact value at $C \simeq 0.5$, but while the damping is strong enough in the corresponding shorter waves to prevent their unstable numerical growth. Then for $C \gtrsim 0.5$ the trend reverses and hence a new shorter waves cycle begins having a numerical propagation speed larger than the physical one, but moving again closer to the physical one with increasing C's. Again this leads to that the instantaneous velocity flips sign once the same threshold is again reached, when the numerical speed again reaches exact value at $C = 1$, which is nondamping implying, the late reversing, instability, when the speed of the longer waves exceeds the exact value. More on this later.

Alternatively, from the von Neumann's complementary analysis point of view, the numerical phase component of the Lax-Wendroff growth factor, Eq. (2.82), is given by

$$\phi = \arctan\left(\frac{\Im(G)}{\Re(G)}\right) = \arctan\left[\frac{-C\,\sin(k\Delta x)}{1 - C^2(1 - \cos(k\Delta x))}\right], \tag{2.88}$$

which we show in the left panel of the Fig. 25.

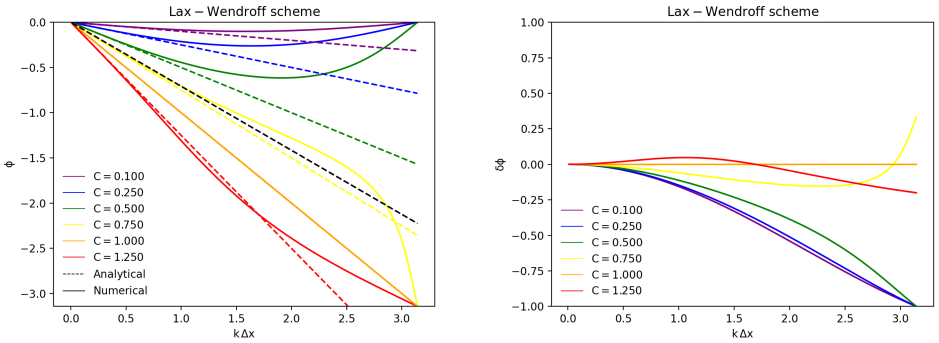

FIGURE 25. Left: the numerical phase component. Right: the numerical relative phase error as a function of phase angle or frequency, in radians, for specific C number values.

Therefore, since the exact phase speed is the $-v$, we present in the right panel of the Fig. 25 the numerical relative phase error (see Eq. (2.30) of Part I) of the Lax-Wendroff scheme plotted against the phase angle for specific C values.

Again in a manner similar to, but not the same as, that which occurs in the Courant-Isaacson-Rees scheme, now the right panel of Fig. 25 shows us, in agreement with findings from 24, that for $C < \sqrt{0.5}$ waves have leading shift but shift closer to the $\delta\phi = 0$ up to a half-dissipation threshold is reached when we have no dispersion error approximately, the relative phase shift error flips sign and the Fourier modes have just the opposite, i.e. lagging shift. Hence only short waves with $C < \sqrt{0.5}$ are poorly resolved, quasi-stationary waves. Nevertheless, for $\sqrt{0.5} < C < 1$ the modes stay in the stable regimen and continue shifting closer to the $\delta\phi = 0$ (see the right panel in Fig. 25) up to the stability threshold is reached when we have no dispersion error exactly, the relative phase shift error flips sign again and the Fourier modes have again leading shift but now driving the solution to instability since, unlike the case when $C = \sqrt{0.5}$, when $C = 1$ the diffusion exactly vanishes and we do reach the analytic solution. In fact, we finally deduce that Eq. (2.79) reduces to $T_j^{n+1} = T_{j-1}^n$ if $C = 1$, the exact solution (see A). The same as the Courant-Isaacson-Rees, Lax's and Wendroff's schemes and also like the Richardson's scheme. Having said all of this, the irregular phase advance found in Fig. 25 (compare this Figure to Fig. 13) is the consequence of the slow dissipation typical for second order explicit schemes as already found in Fig.23.

2.9.5. **Monotonicity.** Finally, from the Eq. (2.38) the coefficients of the new solution are $\frac{1}{2}(C^2 + C)$, $1 - C^2$ and $\frac{1}{2}(C^2 - C)$; the last of which is negative if Eq. (2.84) is satisfied. That is, in the consistency region this Lax-Wendroff scheme behaves non-monotonically, unless C is unity.

2.10. The Molenkamp's 1967 single-step implicit algorithm.

2.10.1. **Construction.** In 1967 Molenkamp [17] considered the same discretization as Courant, Isaaccson and Rees did (Eq. (2.38)), but evaluating the space derivative forwards in time; i.e.,

$$\frac{T_j^{n+1} - T_j^n}{\Delta t} = -v \frac{T_j^{n+1} - T_{j-1}^{n+1}}{\Delta x}, \tag{2.89}$$

which is reformulated in Table 1 using Eq. (2.2).

2.10.2. **Consistency and order of accuracy.** We firstly analyze the consistency of the scheme using the Hirt's method. Substituting each value of T at points other than point (x_j, t^{n+1}) in the scheme in a Taylor

series around the value T_j^{n+1} at that point (x_j, t^{n+1}), i.e. we substitute Eqs. 2.6 and 2.13 of Part I in Eq. (2.89), gives

$$\frac{\partial T}{\partial t} + v\frac{\partial T}{\partial x} = \frac{v\,\Delta x}{2}\frac{\partial^2 T}{\partial x^2} + \frac{\Delta t}{2}\frac{\partial^2 T}{\partial t^2} + \cdots . \tag{2.90}$$

We then see from that equation, which is not yet the modified equation, that the right hand side vanishes when $\Delta t \to 0$ and $\Delta x \to 0$ and therefore the Molenkamp's scheme of calculation is consistent. In addition, this side goes to zero as the first power of Δt and the first power of Δx, implying that the scheme is of first order accuracy in both time and space as well. Indeed, this result further verifies what would otherwise be expected because the way this scheme is based on Taylor series expansions.

We furthermore provide here the evolution equation with only space derivatives, i.e. the modified equation. In order to achieve it, we firstly find expressions for $\frac{\partial^2 T}{\partial t^2}$, and secondly (be careful with this) for $\frac{\partial^3 T}{\partial t^3}$, $\frac{\partial^2 T}{\partial x \partial t}$, $\frac{\partial^3 T}{\partial x^2 \partial t}$ and $\frac{\partial^3 T}{\partial x \partial t^2}$, by differentiating Eq. (2.90); all of which we use systematically to eliminate the time derivatives in it. This implies that the modified equation associated with the Molenkamp's scheme, the equation of the grid function from Molenkamp's difference equation, is:

$$\begin{aligned} &\frac{\partial T}{\partial t} + v\frac{\partial T}{\partial x} \\ &= \left(\frac{C^2 + C}{2}\right)\frac{(\Delta x)^2}{\Delta t}\frac{\partial^2 T}{\partial x^2} + \left(\frac{-C - 3\,C^2 - 2\,C^3}{6}\right)\frac{(\Delta x)^3}{\Delta t}\frac{\partial^3 T}{\partial x^3} + \mathcal{O}((\Delta x)^4), \end{aligned} \tag{2.91}$$

which is one of two ways to next not only calculate the local error but also estimate the stability.

2.10.3. **Stability.** We secondly now analyze the stability using the von Neumann's method. Substituting a term of Eq. (2.1) of Part I into each term a term in Eq. (2.89) we get the following complex valued, growth factor associated with the Molenkamp's scheme:

$$G = \frac{1}{1 + C - C\,\cos(k\Delta x) + i\,C\sin(k\Delta x)}, \tag{2.92}$$

whose magnitude component takes the form

$$|G|^2 = \frac{1}{1 + 2\,C\,(1 + C)\,[1 - \cos(k\Delta x)]} \leq 1, \tag{2.93}$$

which satisfies Eq. (2.16) of Part I and thus the Molenkamp's scheme is stable for the advection equation, as every other implicit scheme.

Alternatively, the modified equation is another way to obtain this. The first (even) term on the right hand of Eq. (2.91), which acts as a diffusion term, always is positive implying that the Molenkamp's scheme is indeed unconditionally stable.

2.10.4. **Accuracy.** We thirdly investigate how accurate, both in magnitude and in phase, the numerical solution is using the Hirt's and von Neumann's complementary analysis.

On the one hand, by applying the discrete Fourier series grid solution of Eq. (2.1) of Part I to the Molenkamp's modified equation (2.91) truncated up to the fourth-order derivatives we see that the damping term of the numerical solution, which is one order of magnitude larger than its dispersion, is not unity as it should be but it is given by

$$\exp\left[\left(\frac{-C-C^2}{2}\right)\frac{(\Delta x)^2}{\Delta t}\,k^2\,\Delta t\right], \tag{2.94}$$

which is shown in left panel of Fig. 26.

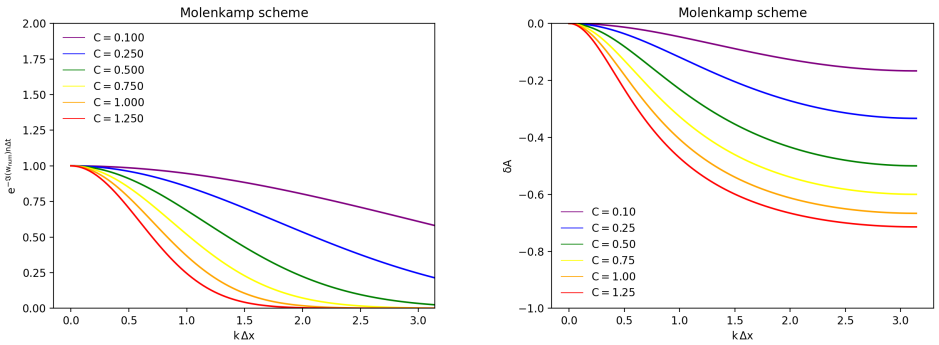

FIGURE 26. Damping factor (approximated to the four-order derivatives) and relative amplitude error as a function of phase angle or frequency, in radians, for specific C number values.

Alternatively, since the exact growth factor is equal to unity, the relative amplitude error (Eq. (2.29) of Part I) is given by

$$\delta A = \frac{1}{\sqrt{1+2\,C\,(1+C)\,[1-\cos\,(k\Delta x)]}} - 1, \tag{2.95}$$

as shown in right panel of Fig. 26. This panel shows that it decreases rapidly (typical for first order schemes) from 0 at $k\Delta x = 0$ (for consistency reasons) when the frequency increases, i.e. the Molenkamp's scheme is uniformly quite dissipative.

On the other hand, by applying the discrete Fourier series grid solution of Eq. (2.1) of Part I to the Molenkamp's modified equation (2.91) truncated up to the fourth-order derivatives, then we see that the dispersive term is given by

$$\exp\left\{i\,k\,\left[x - v\,t + \left(\frac{C + 3\,C^2 + 2\,C^3}{6}\right)\frac{(\Delta x)^3}{\Delta t}\,k^2\,t\right]\right\}, \tag{2.96}$$

implying the dispersive phase velocity shown in Fig. 27. We now find a numerical propagation speed smaller than the physical one, but moving away from the physical one with increasing C's. This leads to the fact that the instantaneous velocity does not flip sign because the numerical speed never reaches exact value, implying the Molenkamp's scheme don't have instability issue. More on this later.

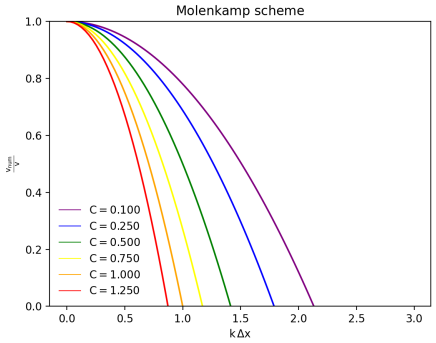

FIGURE 27. The phase velocity of the Molenkamp's solution (approximated to the four-order derivatives), Eq. (2.96) vs. frequency in radians, for specific C values which are distinguished by line colors.

Alternatively, from the von Neumann's complementary analysis point of view, the numerical phase component of the Molenkamp's growth factor, Eq. (2.92), is given by

$$\phi = \arctan\left(\frac{\Im(G)}{\Re(G)}\right) = \arctan\left[\frac{-C\sin(k\Delta x)}{1 + C(1 - \cos(k\Delta x))}\right], \tag{2.97}$$

which we show in the left panel of the Fig. 28.

Therefore, since the exact phase speed is the $-v$, we present in the right panel of the Fig. 28 the numerical relative phase error (see Eq. (2.30) of Part I) of the Molenkamp's scheme plotted against the phase angle for specific C values.

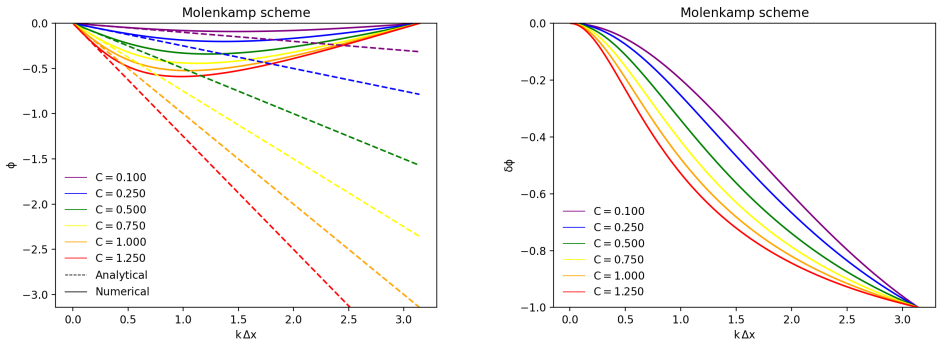

FIGURE 28. Left: the numerical phase component. Right: the numerical relative phase error as a function of phase angle or frequency, in radians, for specific C number values.

We find that the (dispersive) behavior is similar to but more pronounced than those using the Laasonen's, Crank-Nicolson and Lax-Richtmyer schemes. Indeed, the left panel of Fig. 28 shows us that for all values of C we have leading shift, the relative phase error is less than 0, indicating a poorly resolved, numerical propagation speed smaller than the physical one; but shift away from the line $\delta\phi = 0$ (see the left panel of Fig. 28), implying again the Molenkamp's scheme don't have instability issue, either. Also, let us not forget that the dissipative behavior is much worse than those of the Crank-Nicolson and Laasonen's schemes and similar to that of Lax-Richtmyer scheme.

2.10.5. **Monotonicity.** Since the Molenkamp's scheme is implicit the convex combination technique fails to estimate its monotonicity. Therefore we must demonstrate Eq. (2.31) of Part I. From Eq. (2.89) (see Table 1) we also get

$$-C\,T_{j-2}^{n+1} + T_{j-1}^{n+1} + C\,T_{j-1}^{n+1} = T_{j-1}^{n}, \tag{2.98}$$

which subtracted from Eq. (2.89) gives

$$T_j^{n+1} - T_{j-1}^{n+1} = T_j^n - T_{j-1}^n - C\,(T_{j-1}^{n+1} - T_j^{n+1}) + C\,(T_j^{n+1} - T_{j-1}^{n+1}); \tag{2.99}$$

and if in this equation we take the absolute value of both sides, use the triangle inequality on the right-side and sum the two sides over all j then we get Eq. (2.31) of Part I. Hence, the Molenkamp's scheme is monotone and does not introduce oscillations.

2.11. **The Lerat's 1979 single-step implicit algorithm.**

2.11.1. **Construction.** In 1979 Lerat [18] considered the same discretization as Lax and Wendroff did (Eq. (2.79)), but evaluating the space derivatives forwards in time; i.e.,

$$T_j^{n+1} = T_j^n - \Delta t\, v\, \frac{T_{j+1}^{n+1} - T_{j-1}^{n+1}}{2\Delta x} + \frac{1}{2}(\Delta t)^2\, v^2\, \frac{T_{j-1}^{n+1} - 2T_j^{n+1} + T_{j+1}^{n+1}}{(\Delta x)^2} + \mathcal{O}\left((\Delta t)^2 + \frac{(\Delta x)^2}{\Delta t} + (\Delta x)^2\right), \tag{2.100}$$

which is reformulated in Table 1 using Eq. (2.2).

2.11.2. **Consistency and order of accuracy.** We firstly analyze the consistency of the scheme using the Hirt's method. Substituting each value of T at points other than point (x_j, t^{n+1}) in the scheme in a Taylor series around the value T_j^{n+1} at that point (x_j, t^{n+1}), i.e. we substitute Eqs. 2.8, 2.12 and 2.13 of Part I in Eq. (2.100), gives

$$\frac{\partial T}{\partial t} + v\frac{\partial T}{\partial x} = \frac{v^2\,\Delta t}{2}\frac{\partial^2 T}{\partial x^2} + \frac{\Delta t}{2}\frac{\partial^2 T}{\partial t^2} - \frac{v\,(\Delta x)^2}{6}\frac{\partial^3 T}{\partial x^3} - \frac{(\Delta t)^2}{6}\frac{\partial^3 T}{\partial t^3} + \cdots. \tag{2.101}$$

We then see from that equation, which is not yet the modified equation, that the right hand side vanishes when $\Delta t \to 0$ and $\Delta x \to 0$ and therefore the Lerat's scheme of calculation is consistent. In addition, this side goes to zero as the first power of Δt and the second power of Δx, implying that the scheme is of first order accuracy in time and second order accuracy in space as well. Indeed, this result further verifies what would otherwise be expected because the way this scheme is based on Taylor series expansions.

We furthermore provide here the evolution equation with only space derivatives, i.e. the modified equation. In order to achieve it, we firstly find expressions for $\frac{\partial^2 T}{\partial t^2}$ and $\frac{\partial^3 T}{\partial t^3}$, and secondly (be careful with this) for $\frac{\partial^2 T}{\partial x \partial t}$, $\frac{\partial^3 T}{\partial x^2 \partial t}$ and $\frac{\partial^3 T}{\partial x \partial t^2}$, by differentiating Eq. (2.101); all of which we use systematically to eliminate the time derivatives in it. This implies that

the modified equation associated with the Lerat's scheme, the equation of the grid function from Lerat's difference equation, is:

$$\frac{\partial T}{\partial t}+v\frac{\partial T}{\partial x}=\frac{(\Delta x)^2}{\Delta t}\,C^2\frac{\partial^2 T}{\partial x^2}+\left(\frac{-C-5\,C^3}{6}\right)\frac{(\Delta x)^3}{\Delta t}\frac{\partial^3 T}{\partial x^3}+\mathcal{O}((\Delta x)^?), \tag{2.102}$$

which is one of two ways to next not only calculate the local error but also estimate the stability.

2.11.3. **Stability.** We secondly now analyze the stability using the von Neumann's method. Substituting a term of Eq. (2.1) of Part I into each term a term in Eq. (2.100) we get the following complex valued, growth factor associated with the Lerat's scheme:

$$G=\frac{1}{1+C^2-C^2\,\cos\left(k\Delta x\right)+i\,C\sin\left(k\Delta x\right)}, \tag{2.103}$$

whose magnitude component takes the form

$$|G|^2=\frac{1}{(1+C^2-C^2\,\cos\left(k\Delta x\right))^2+C^2\,\sin^2\left(k\Delta x\right)}\leq 1, \tag{2.104}$$

which satisfies Eq. (2.16) of Part I and thus the Lerat's scheme is stable for the advection equation, as every other implicit scheme.

Alternatively, the modified equation is another way to obtain this. The first (even) term on the right hand of Eq. (2.102), which acts as a diffusion term, has to be positive for T_j^n to be damped in time; which is fulfilled implying that the Lerat's scheme is indeed unconditionally stable.

2.11.4. **Accuracy.** We thirdly investigate how accurate, both in magnitude and in phase, the numerical solution is using the Hirt's and von Neumann's complementary analysis.

On the one hand, by applying the discrete Fourier series grid solution of Eq. (2.1) of Part I to the Lerat's modified equation (2.102) truncated up to the fourth-order derivatives we see that the damping term of the numerical solution, which is one order of magnitude larger than its dispersion, is not unity as it should be but it is given by

$$\exp\left[-C^2\,\frac{(\Delta x)^2}{2\,\Delta t}\,k^2\,\Delta t\right], \tag{2.105}$$

which is shown in left panel of Fig. 29.

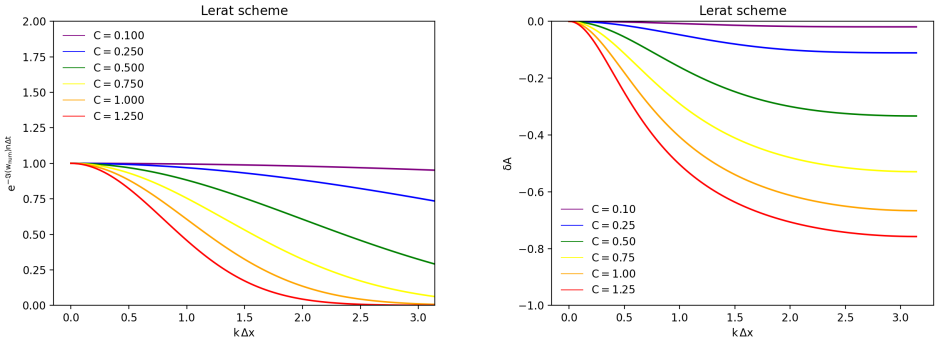

FIGURE 29. Damping factor (approximated to the four-order derivatives) and relative amplitude error as a function of phase angle or frequency, in radians, for specific C number values.

Alternatively, since the exact growth factor is equal to unity, the relative amplitude error (Eq. (2.29) of Part I) is given by

$$\delta A = \frac{1}{\sqrt{(1 + C^2 - C^2\,\cos\,(k\Delta x))^2 + C^2\,\sin^2\,(k\Delta x)}} - 1, \qquad (2.106)$$

as shown in right panel of Fig. 29. This panel shows that it decreases rapidly (typical for first order schemes) from 0 at $k\Delta x = 0$ (for consistency reasons) when the frequency increases, i.e. the Lerat's scheme is uniformly dissipative. The same as that which occurs in the Molenkamp's scheme.

On the other hand, by applying the discrete Fourier series grid solution of Eq. (2.1) of Part I to the Lerat's modified equation (2.102) truncated up to the fourth-order derivatives, then we see that the dispersive term is given by

$$\exp\left\{i\,k\,\left[x - v\,t + \left(\frac{C + 5\,C^3}{6}\right)\frac{(\Delta x)^3}{\Delta t}\,k^2\,t\right]\right\}, \qquad (2.107)$$

implying the dispersive phase velocity shown in Fig. 30. We now find a numerical propagation speed smaller than the physical one, but moving away from the physical one with increasing C's. This leads to the fact that the instantaneous velocity does not flip sign because the numerical speed never reaches exact value, implying the Lerat's scheme don't have instability issue. More on this later.

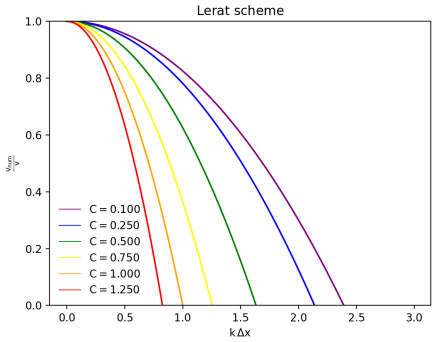

FIGURE 30. The phase velocity of the Lerat's solution (approximated to the four-order derivatives), Eq. (2.107) vs. frequency in radians, for specific C values which are distinguished by line colors.

Alternatively, from the von Neumann's complementary analysis point of view, the numerical phase component of the Lerat's growth factor, Eq. (2.103), is given by

$$\phi = \arctan\left(\frac{\Im(G)}{\Re(G)}\right) = \arctan\left[\frac{-C\sin(k\Delta x)}{1+C^2[1-\cos(k\Delta x)]}\right], \tag{2.108}$$

which we show in the left panel of the Fig. 31.

Therefore, since the exact phase speed is the $-v$, we present in the right panel of the Fig. 31 the numerical relative phase error (see Eq. (2.30) of Part I) of the Lerat's scheme plotted against the phase angle for specific C values.

We find that the (dispersive) behavior is quite similar to but even more pronounced as that which occurs in the Molenkamp's scheme. Indeed, the left panel of Fig. 31 shows us that for all values of C we have leading shift, the relative phase error is less than 0, indicating a poorly resolved, numerical propagation speed smaller than the physical one; but shift away from the line $\delta\phi = 0$ (see the left panel of Fig. 31), implying again the Lerat's scheme don't have instability issue, either.

2.11.5. **Monotonicity.** Since the Lerat's scheme is implicit the convex combination technique fails to estimate its monotonicity. Therefore we must demonstrate Eq. (2.31) of Part I. From Eq. (2.100) (see Table 1) we also get

$$-0.5\,C^2\,T_{j-2}^{n+1} - 0.5\,C\,T_{j-2}^{n+1} + T_{j-1}^{n+1} + C^2\,T_{j-1}^{n+1}$$

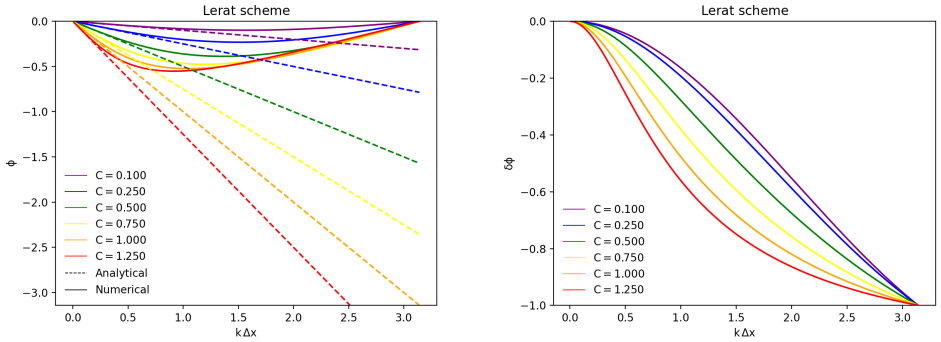

FIGURE 31. Left: the numerical phase component. Right: the numerical relative phase error as a function of phase angle or frequency, in radians, for specific C number values.

$$-0.5\,C^2\,T_j^{n+1} + 0.5\,C\,T_j^{n+1} = T_{j-1}^n, \tag{2.109}$$

which subtracted from Eq. (2.100) gives

$$\begin{aligned} T_j^{n+1} - T_{j-1}^{n+1} = T_j^n - T_{j-1}^n + 0.5\;C^2\,(T_{j-1}^{n+1} - T_j^{n+1}) + 0.5\;C\,(T_{j-1}^{n+1} - T_j^{n+1}) \\ + 0.5\;C^2\,(T_{j+1}^{n+1} - T_j^{n+1}) - 0.5\;C\,(T_{j+1}^{n+1} - T_j^{n+1}) \\ + C^2\,(T_j^{n+1} - T_{j-1}^{n+1}); \end{aligned} \tag{2.110}$$

and if in this equation we take the absolute value of both sides, use the triangle inequality on the right-side and sum the two sides over all j then we get Eq. (2.31) of Part I. Hence, the Lerat's scheme is monotone and does not introduce oscillations.

3. **The numerical tests**

The critical properties of the depending on time instantaneous grid function for a basic example and proxy for the presence of unsmooth initial conditions are explored in this experimental Section, as testbed for detailed fundamentals and practice quantitatively predicted in the previous section. In particular, equipped with a analytical solution, we critically assess the performance, in terms of stability, accuracy, and also convergence, of different numerical solution schemes to solve the diffusion. Comparisons with each other are finally commented.

More specifically, the illustrative application we use is the Lagrange-Charpit 1776 analytical solution of the representative and challenging Cauchy problem described in the A on bounded domain size $L = 1$,

initial condition given in Eq. (A.1) and speed $v = 1$ arbitrary units, which deals with evolving discontinuous derivatives in solution quantity. So, by choosing a mean best-fit resolution, the full parameter space of every discretization model, summarized in Table 2, is validated (or otherwise) and compared to exact solution and other numerical solutions with special emphasis on graphical exposition.

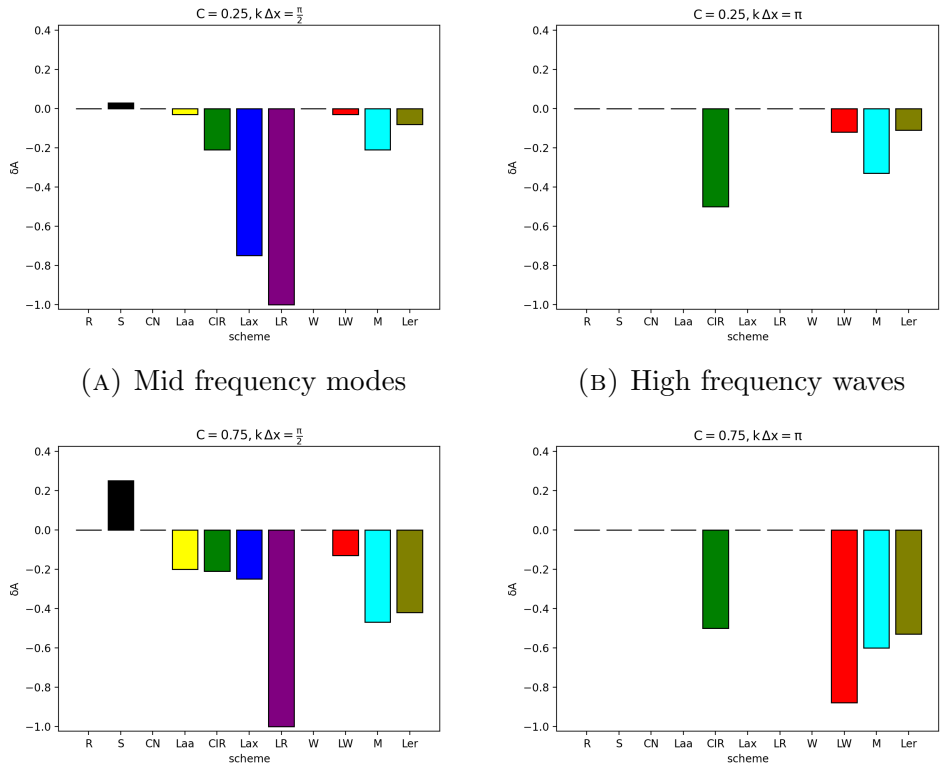

(A) Mid frequency modes

(B) High frequency waves

(C) Mid frequency waves

(D) High frequency waves

FIGURE 32. Amplitude errors of different schemes for some values of the dimensionless Courant-Friedrichs-Lewy number, Eq. (2.2) (i.e. different discretisations). In the diffusion, upper panels we show the Schmidt's scheme by its black bar.

For the sake of comparison, we represent both dissipation and dispersion errors representative of the schemes for two specific C values in Figs. 32 and 33, respectively. Although we know the numerical error depends on the precise combination of time stepping scheme and finite difference,

Table 2: Parameter space of the schemes analysed in this work, including the unstable Schmidt's scheme.

Author	Order	Stability	Next-to-leading accuracy		Oscillations
			Dissipation coefficient	Dispersion coefficient	
Richardson [6]	$\mathcal{O}((\Delta t)^2 + (\Delta x)^2)$	$C \leq 1$	0	$\frac{1}{6}(-C + C^3)\frac{(\Delta x)^3}{\Delta t}$	Yes
Schmidt [8]	$\mathcal{O}(\Delta t + (\Delta x)^2)$	Unstable	$+\frac{1}{2}C^2\frac{(\Delta x)^2}{\Delta t}$	$\frac{1}{6}(C + 2\,C^3)\frac{(\Delta x)^3}{\Delta t}$	Yes
Crank-Nicolson [9]	$\mathcal{O}((\Delta \mathrm{t})^2 + (\Delta \mathrm{x})^2)$	Stable	0	$\frac{1}{6}\left(-C + \frac{C^3}{4}\right)\frac{(\Delta x)^3}{\Delta t}$	Yes
Laasonen [11]	$\mathcal{O}(\Delta t + (\Delta x)^2)$	Stable	$-\frac{1}{2}C^2\frac{(\Delta x)^2}{\Delta t}$	$\frac{1}{6}(-C - 2\,C^3)\frac{(\Delta x)^3}{\Delta t}$	No
Courant-Isaccson-Rees [12]	$\mathcal{O}(\Delta t + \Delta x)$	$C \leq 1$	$-\frac{1}{2}(C - C^2)\frac{(\Delta x)^2}{\Delta t}$	$\frac{1}{6}(-C + 3\,C^2 - 2\,C^3)\frac{(\Delta x)^3}{\Delta t}$	No
Lax [13]	$\mathcal{O}(\Delta t)$	$C \leq 1$	$-\frac{1}{2}(1 - C^2)\frac{(\Delta x)^2}{\Delta t}$	$\frac{1}{6}(2\,C - 2\,C^3)\frac{(\Delta x)^3}{\Delta t}$	No
Lax-Richtmyer [14]	$\mathcal{O}(\Delta t + (\Delta x)^2)$	Stable	$-\frac{1}{2}C^2\frac{(\Delta x)^2}{\Delta t}$	$\frac{1}{6}(-C - 2\,C^3)\frac{(\Delta x)^3}{\Delta t}$	No
Wendroff [15]	$\mathcal{O}((\Delta t)^2 + (\Delta x)^2)$	Stable	0	$\frac{1}{6}\left(\frac{C - C^3}{4}\right)\frac{(\Delta x)^3}{\Delta t}$	Yes
Lax-Wendroff [16]	$\mathcal{O}((\Delta t)^2 + (\Delta x)^2)$	$C \leq 1$	$-\frac{1}{8}(C^2 - C^4)\frac{(\Delta x)^4}{\Delta t^2}$	$\frac{1}{6}(-C + C^3)\frac{(\Delta x)^3}{\Delta t}$	Yes
Molenkamp [17]	$\mathcal{O}(\Delta t + \Delta x)$	Stable	$-\frac{1}{2}(C + C^2)\frac{(\Delta x)^2}{\Delta t}$	$\frac{1}{6}(-C - 3\,C^2 - 2\,C^3)\frac{(\Delta x)^3}{\Delta t}$	No
Lerat [18]	$\mathcal{O}(\Delta \mathrm{t} + (\Delta \mathrm{x})^2)$	Stable	$-\frac{1}{2}C^2\frac{(\Delta x)^2}{\Delta t}$	$\frac{1}{6}(-C - 5\,C^3)\frac{(\Delta x)^3}{\Delta t}$	No

the marked differences between each method and its implicit version are outstanding just by looking at the Schmidt's bars vs. Laasonen, Lax's bars vs. Lax-Richtmyer, Courant-Isaccson-Rees bars vs. Molenkamp and Lax-Wendroff bars vs. Lerat.

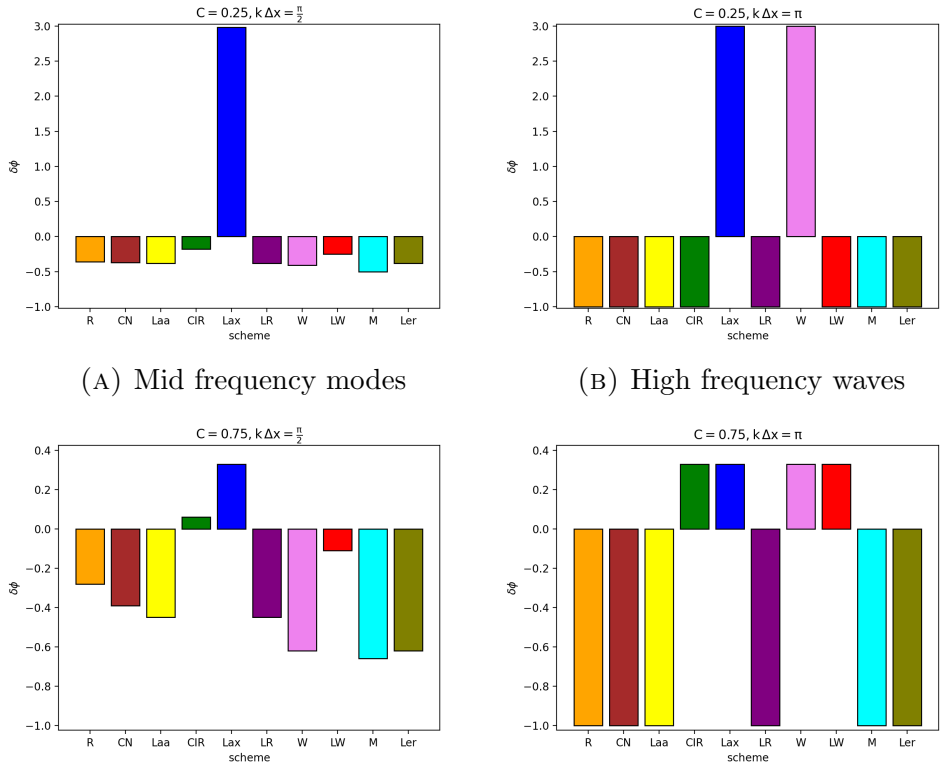

(A) Mid frequency modes

(B) High frequency waves

(C) Mid frequency modes

(D) High frequency waves

FIGURE 33. Phase errors of different schemes for some values of the dimensionless Courant-Friedrichs-Lewy number, Eq. (2.2) (i.e. different discretisations). In the diffusion, upper panels we show the Schmidt's scheme by its black bar.

Finally, we remind that included in our sample is a no go condition using the Schmidt's scheme and some problematic strictures with respect to the usage of both the Richardson's scheme and Lax-Richtmyer scheme and with the Lax's scheme, as well as the inability to use a large time step in all cases. This latter is for the Courant-Friedrichs-Lewy condition

in explicit cases, accuracy in nonexplicit cases and additionally consistency in Lax's case. In this context and with all these central questions in mind, to gain a better understanding of different subtleties creating their signatures, before anything else, we demonstrate how to perform frequentist scheme comparison.

3.1. **Resolution tests.** The present tests aim to constrain the Δt parameter by performing a frequentist error minimization either opening or, in order to resolve the initial condition well, keeping fixed a sufficiently small grid spacing $\Delta x = 10^{-2}$ units.

We compute the heat flow in the unit domain [0, 1] using the Richardson's approximation which likewise lacks its lowest time level evolving its required first time step solution from the simplest Courant-Isaccson-Rees scheme.

To this end, Fig. 34 shows the residuals' behavior obtained for the non unstable, explicit schemes, namely, Richardson's, Courant-Isaacson-Rees, Lax's and Lax-Wendroff schemes and Fig. 35 shows the same for both semi-implicit (namely, Crank-Nicholson, Lax-Richtmyer and Wendroff's schemes) and implicit (namely, Laasonen's, Lerat's and Molemkamp's schemes) schemes. We use the simplest Schmidt's scheme to compute the lowest time level required by the Du Fort-Frankel three-level approximation. The codes naturally take into account the initial condition either in the first iteration, in case of the first row explicit schemes, or in the constant matrix, in other cases.

Our investigation reveals four results of utmost importance. First, the stable schemes (see Fig. 35) produce higher error with the use of larger values of C. This would seem in apparent contradiction to unconditionally stable non-explicit schemes at first glance.

Second, the second-order schemes, namely, Richardson's, Lax-Wendroff, Crank-Nicholson and also Wendroff's schemes, are more accurate but not about one order of magnitude more accurate simply a factor of about three better.

Third, the Crank-Nicholson scheme exhibits the smallest variation with C.

Fourth, most of schemes, except Courant-Isaacson-Rees, Lax's and Lax-Richtmyer schemes where the opposite is true, produce less error with a lower value of time step. Furthermore, we also find that this result holds for a finer spatial resolution. For example, let's take the case shown in Fig. 36 corresponding to Lax-Wendroff scheme with 200

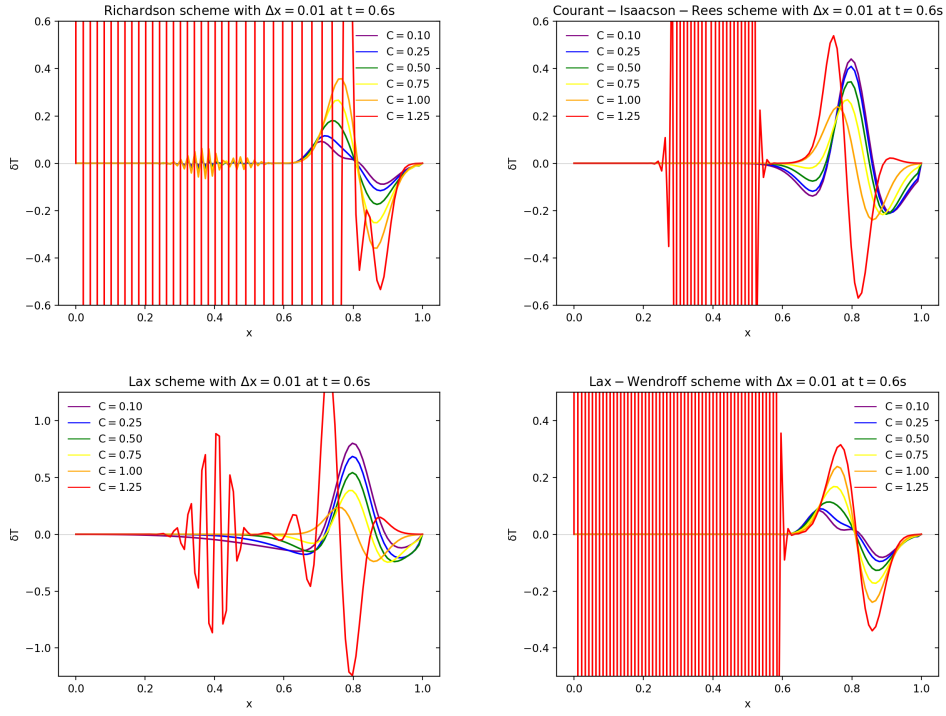

FIGURE 34. Errors of explicit schemes for some values of the dimensionless Courant-Isaacson-Rees number, Eq. (2.2) (i.e. different scheme resolution).

gridpoints, i.e. with twice the resolution of the one computed with the same scheme and shown in the last panel of Fig. 34.

Fifth, the schemes that are exact for a $C = 1$, namely, Richardson's, Courant-Isaacson-Rees, Lax's, Wendroff's and Lax-Wendroff, are not noticed.

Here we offer the following four respective explanations.

- First, the solution to this puzzle is principally the strong dispersion suffered by these schemes. Indeed, this result is a consequence of the behavior illustrated in Figs. 7, 16, 19, 22, 28 and 31 each. In addition to this, the Lax-Richtmyer scheme stands out with the worse error, which is due to its much stronger dissipation (see Fig. 17).

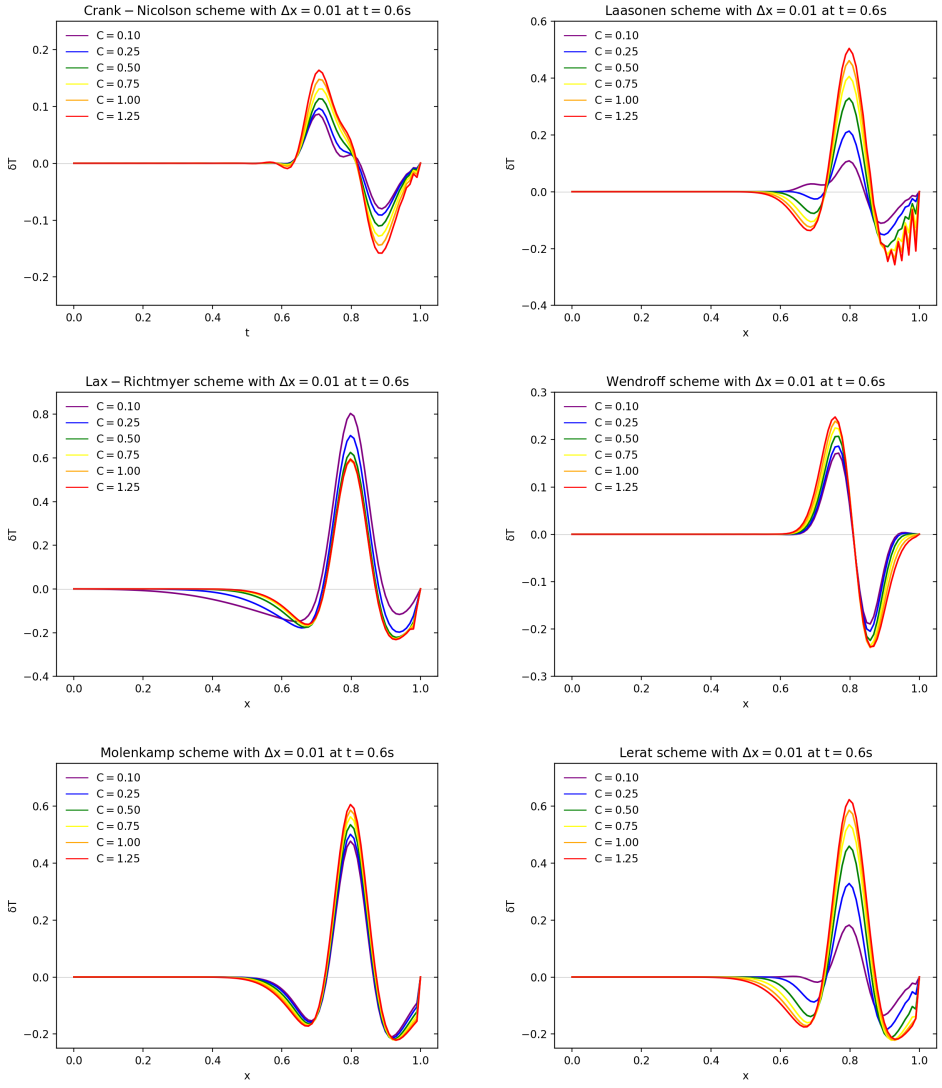

FIGURE 35. The same as Fig. 34 but for non-explicit schemes including both semi-implicit ones (the first three) and implicit ones (the last three).

- Second, Godunov's oscillations we already explained in Section 2.2.4 in Part I. In the second order schemes always appear non-physical oscillations, especially for our initial Gaussian data (see A) as we shall discuss shortly.

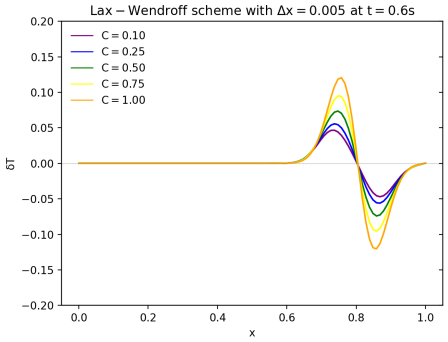

FIGURE 36. The same as Fig. 34 but for Lax-Wendroff scheme with 200 gridpoints.

- Third, here we observe the evidence in Fig. 7 that the Crank-Nicholson relative phase is very little affected by the value of C, along with their non-damping amplitude.
- Third, transport errors we now explain for the first time. We observe in Table 1 that there are three schemes where the evolution of the solutions is markedly assymetrical. They are the Courant-Isaacson-Rees, Lax's and Lax-Richtmyer schemes. For example the value of T_j^n has no influence on T_j^{n+1} in the Lax's and Lax-Richtmyer schemes, which causes the schemes to lose stability and the accuracy condition ($C = 1$ for all of them) ends up dominating the evolution. In this way they show the counter-intuitive behavior we find here. In addition to this, the Lax's and Lax-Richtmyer schemes stand out with the worse errors, which is due to their much stronger dissipation of well resolved waves (see Figs. 14 and 17).

  Moreover, in addition to them, Richardson's, Wendroff's and Molenkamp's schemes are weakly assymetrical but, still, it is not enough for poor accuracy to dominate the propagation and get worse with larger C values.
- Fourth, we are finding that an appreciable error from the discretization of the initial Gaussian data is present in our application. More details will be given in Section 3.4.

Consequently, based on this graphical statistical evidence and at the same time with the awareness of both the stability and accuracy limitations and with the Lax's consistency limitation, we agree to carefully

choose the simultaneous most accurate discretization of $C = 0.5$ from visual inspection of Figs. 34 and 35, i.e. a time increment of half a order of magnitud smaller than the acceptable spatial resolution of 10^{-2} units. In fact, resolving the abrupt initial and boundary conditions require time to reach described accuracy, and potentially explains our choice. In other words, this subsection explains why the precision of the solution does not only depend on the numerical resolution, but also on the temperature quantity gradient as will be checked later.

The advantage of this natural approach is that all schemes can be used on an equal footing. The caveat is that individual peculiarities are averaged out. Nonetheless, as previously anticipated, Fig. 35 illustrates that the stability benefit of the non-explicit schemes, consisting only in that we may use (and save computing time with) a large Δt parameter, does not keep against this differencial equation. The same as in Part I.

3.2. **Stability tests.** We are now able to extend that Section in three directions. We firstly demonstrate the stability of different schemes.

3.2.1. **Unstable scheme.** Fig. 4 shows certainly that the Schmidt's scheme amplify errors for all the Courant-Isaacson-Rees number values, i.e. δA is everywhere larger or equal 0.

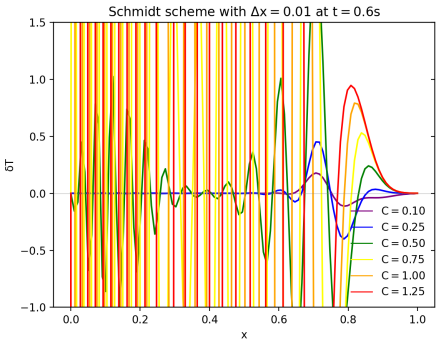

FIGURE 37. The same as Fig. 34 but for Schmidt's (1924) scheme.

Likewise Fig. 37 shows the unacceptable residuals computed with it as a consequence of its instability, as explained in Section 2.2.

Finally, in proof of agreement with Section 2.2, the upper panel of Fig. 38 shows certainly that the Schmidt's scheme amplifies errors and diverges very rapidly. The onset of instability occurs before $t = 0.05$ units

and then only gets worse. The size of the prediction error, measured in RMSE or standard deviation of the residuals (lower panel of Fig. 38), is about two orders of magnitude greater than acceptable even at this early stages. We also find that it makes no difference with any other choice of the grid size. Therefore, we cannot use the Schmidt's scheme to solve any hyperbolic partial differential equation (see third paper in the series).

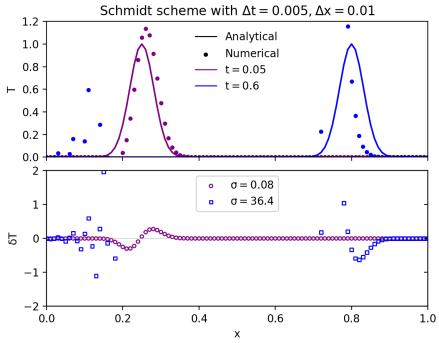

FIGURE 38. The Schmidt's (1910) scheme. Top panel: $T_i^{0.05}$ (violet open circles: ○) and $T_i^{0.6}$ (blue circles: ○) for the Schmidt's (1924) scheme with $\Delta x = 10^{-2}$ and $\Delta t = 5 \times 10^{-3}$. The corresponding solid lines reproduce $T(x, 0.05)$ (violet) and $T(x, 0.6)$ (blue) from Eq. (A.2). Bottom panel shows residual temperatures for the grid points. The legend in the lower panel displays the Root Mean Squared Error, RMSE, for each time.

3.2.2. **Conditionally stable, explicit schemes.** Fig. 11 reveals the conditional stability of the Courant-Isaacson-Rees scheme. The same is shown by Figs. 14 and 23 in the cases of Lax's and Lax-Wendroff schemes, respectively.

Fig. 34 clearly show the same, including the Richardson's scheme—which has no diffusion error as shown in Fig. 1. Specifically, we observe that all these explicit schemes start to wildly oscillate when we apply them with $C > 1$, i.e. they cannot be used when $C > 1$. Even the Richardson's scheme with $C = 1$ shows spurious oscillations due to its computational (numerical) mode.

3.2.3. **Stable, non-explicit schemes.** Fig. 8 reveals the unconditional stability of the Laasonen's scheme. The same is shown by Figs. 17, 26

and 29 in the cases of Lax-Richtmyer, Molenkamp's and Lerat's schemes, respectively.

Fig. 35 clearly show the same, including both the Crank-Nicolson and Wendroff's schemes—which have no diffusion errors as shown in Figs. 5 and 20.

3.3. **Accuracy tests.** We secondly demonstrate the accuracy of different schemes. To achieve this, we present in Fig. 39 the results we obtain for the first order schemes, namely, Courant-Isaacson-Rees, Lax's, Lax-Richtmyer, Laasonen's, Molemkamp's and Lerat's schemes. Fig. 40 presents the results obtained for the second order schemes, namely, Crank-Nicholson, Lax-Wendroff, Lax-Richtmyer and Wendroff's schemes.

According to what we already have worked in Section 3.1 we use the parameters $\Delta x = 10^{-2}$ spatial units and $\Delta t = 5 \times 10^{-3}$ temporal units (already done in Fig. 38).

3.3.1. **First order schemes.** Our investigation reveals six important results. First, no scheme shows oscillations.

Second, all the schemes show a sharp decrease in amplitude. Specifically, the Lax's and Molemkamp's numerical solutions are the most strongly damped. Interestingly, the same as the Lax-Richtmyer scheme.

Third, the Lax's numerical solution leads the exact solution. Surprisingly, it seems to be the same with the Lax-Richtmyer scheme but a closer look to it shows that it is not so.

Fourth, the Courant-Isaacson-Rees, Lax's and Lax-Richtmyer numerical solutions are assymetric.

Fifth, there is hardly difference between explicit and implicit schemes. For example, let us compare the Courant-Isaacson-Rees scheme vs. Molemkamp's scheme on the one hand, but also the Lax's scheme versus Lax-Richtmyer scheme on the other hand.

Sixth, the Laasonen's scheme is the more accurate scheme, followed by the Lerat's scheme and, interestingly enough but not too surprisingly, followed in third place by the Courant-Isaacson-Rees scheme.

Here we offer the following six respective explanations.

- We are showing the Godunov's theorem [5]. The linear monotone schemes for the advective transport can be only first order schemes whilst the second order schemes always present artificial wiggles into their solutions.

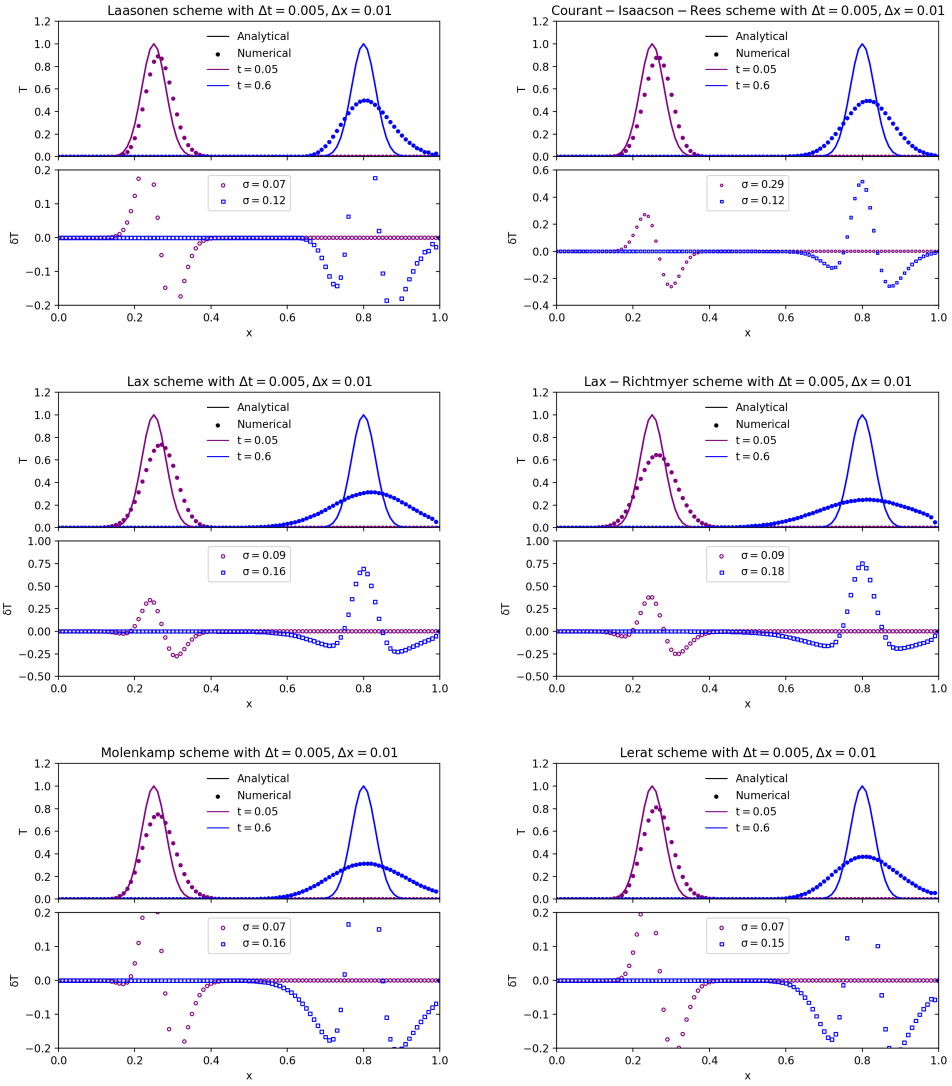

FIGURE 39. The same as Fig. 38 but for all of first order schemes in the sample, including the Lax' scheme.

- This is due to the selectively dissipative behaviors found in Figs. 8, 14 and 17 and, likewise, to the uniformly dissipative behaviors of Figs. 11, 26 and 29. In fact, we have found (see also both the Table 2 and the Fig. 32) that the highest dissipation coefficient is that in the Lax-Richtmyer scheme, followed by the Lax's and Molemkamp's schemes in order of intensity, as is evident in the

Fig. 39. The Molemkamp's scheme is almost indistinguishable from the Lerat's scheme, but its dissipation is stronger.

- We find that the numerical solution of almost all schemes lag behind the exact solution. The reason is that the relative dispersion error is mostly negative as we have found in the above Section. Indeed, we found in Eq. (2.58) and showed in the Fig. 15 that the numerical solution of the Lax's scheme is the only first-order solution leading the exact solution, implying what is observed on the left panel in the second row in this Fig. 39 due to his leading phase error.
- We are finding the transport errors, we put forward just above, in these three schemes.
- If, with the help of Table 2, we compare the two types of schemes of the same order of accuracy, e.g. Courant-Isaacson-Rees scheme vs. Molemkamp's scheme, then we observe the two coefficients, of dissipation and of dispersion, are very similar. Likewise, the same is true when we compare the Lax's scheme and its implicit version, the Lax-Richtmyer scheme.
- This is due to these two Laasonen's and Lerat's schemes have the lowest dissipation of all first-order schemes (see also their dissipation coefficients in the Table 2). What naturally happens is that the Lerat's dispersion error is greater than that of Laasonen.

  Here it is worth emphasizing the superiority of the von Neumann's method to discern the stronger dissipation of the Lax-Richtmyer scheme versus the Laasonen's scheme despite their similarity according to the Hirt's method, at least up to low order.

  Also, we note here that the Courant-Isaacson-Rees diffusion error achieves its maximum value for $C = 0.5$, which makes our choice a less favorable choice to it.

3.3.2. **Second order schemes.** Our investigation reveals five important results. First, all the schemes produce (spurious) oscillations in their numerical solution.

Second, the second-order schemes are not dissipative and, consequently, more accurate.

Third, Wendroff's numerical solution leads the exact solution.

Fourth, there is hardly difference between explicit and semi-explicit schemes. For example, let's compare Lax-Wendroff scheme vs. Crank-Nicholson scheme.

Fifth, the Lax-Wendroff scheme is the more accurate scheme.

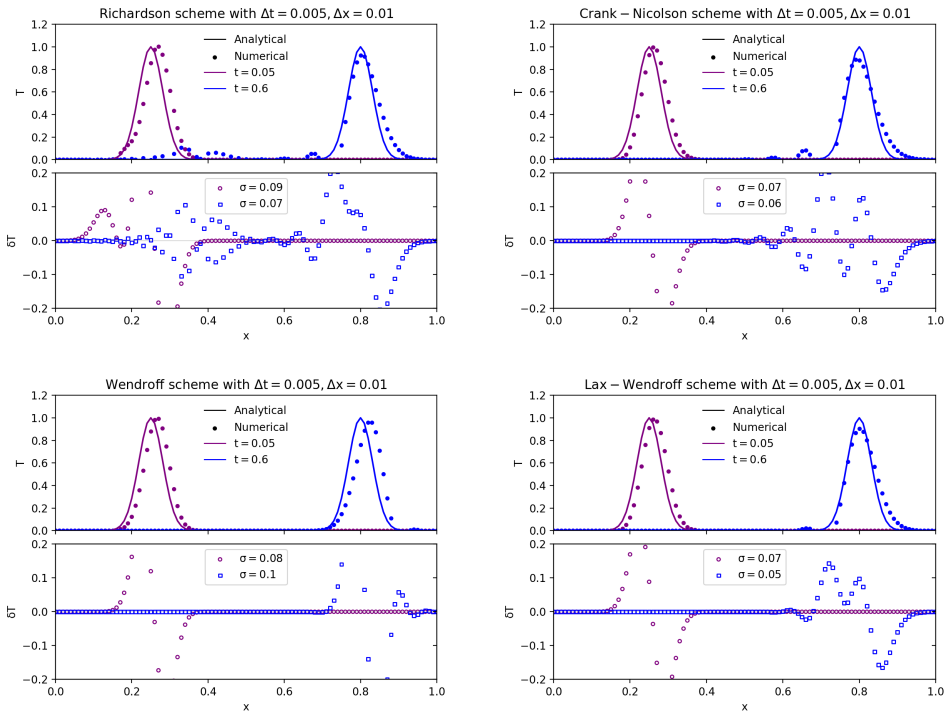

FIGURE 40. The same as Fig. 38 but for all of second order schemes of the sample.

Here we offer the following five respective explanations.

- They are the consequence of the non monotonicity of these two schemes. We are demonstrating the Godunov's theorem [5] (compare Fig. 39 to Fig. 40).
- Due to symmetry, higher-order even derivatives cancel out to eliminate algorithmic dissipation. Compare Fig. 39 to Fig. 40 to confirm their accuracies.
- As we have emphasize just above, the reason is that its relative dispersion error is negative. As found in Eq. (2.76) and showed in Fig. 21, the Wendroff's relative phase, which is the only second-order solution leading the exact solution, strongly impacts the observed numerical solution on the left panel in the second row in this Fig. 40. Note the extra wiggles that appear in the Wendroff's solution leading the exact curve due to his phase advance error is a leading one.

- If, with the help of Table 2, we also compare the two types of schemes of the same order of accuracy, e.g. Lax-Wendroff scheme vs. Crank-Nicholson scheme, then we observe the two coefficients, of dissipation and of dispersion, are very similar (recall the Lax-Wendroff scheme is of fourth order dissipation).
- This is due to that this Lax-Wendroff scheme have the lowest dispersion of all second-order schemes while it is not widely dissipative using the chosen $C = 0.5$ value (see also their coefficients in Table 2, which still is good at putting any possible inaccuracy right. The Richardson's and Wendroff's schemes, for their parts, suffer from inevitable inaccuracies. As for the Crank-Nicolson scheme, it presents excessive dispersion.

3.4. **Convergence tests.** Lastly, we explore the error convergence of different schemes. In Part I we already have explained that consistency means that the error at each time step goes to zero as the grid is refined and in Section 2 we have estimated the rate that this one-step error goes to zero. Here we investigate global (not local over one time step) rate of convergence, i.e. the overall approximation error.

Fig. 41 re-presents the RMSE errors of both first- (undashed) and second-order (dashed) schemes obtained in Figs. 39 and 40. As we already have discussed, it is unsurprising that no second-order scheme is dissipative. But it is also true that none of them is monotone, as Godunov show us. This is what we are finding and happens without contradiction for our non-smooth numerical solutions.

To investigate the matter further, let us emphasize that Figs. 39 and 40 present the numerical solutions to a problem for which the analytical solution, shown in A, is a Gaussian function with discontinuous derivative at $x = 8$ units ($t = 0.6$ units), i.e. is nonmonotone. In other words, we analyze an analytical Gaussian beam composed of a linear combination of Fourier modes of arbitrarily high frequency and, as we have demonstrated, we do by using numerical schemes just able to poorly resolve a finite number of these modes, up to those in the range $0 \leq k\,\Delta x \leq \pi/2$. Indeed, all ten schemes resolve very poorly their high frequency Fourier harmonics. This fact is very significant in those problems where the initial and boundary condition is a non-smooth continuous function rendering their convergence limited. Additionally, all six first-order schemes also smear the non-smooth analytical solution on the one hand, and all four second-order schemes also introduce additional algorithmic oscillations on the other hand. Consequently, we do not obtain for none of them

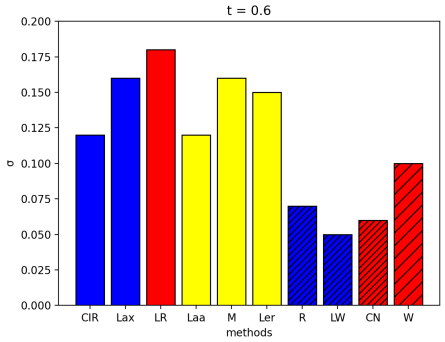

FIGURE 41. Bar plot with the RMSE errors. The blue bars represent explicit schemes, the yellow bars represent fully implicit schemes, the red bars represent semi-explicit schemes and the dashed bars indicate second-order schemes. It suggests that the dashed bars remain viable.

their order of accuracy when we compute the rate of convergence which we do in l^2-norm error (Eq. (2.5) of Part I), and show in Fig. 42. In fact, we observe in Fig. 42 that the second-order schemes are converging at about first order, while the first-order schemes are converging at much less than first order.

Note this finding does not disprove the Lax-Richtmyer theorem [14], because it is only concerning well-posed problems.

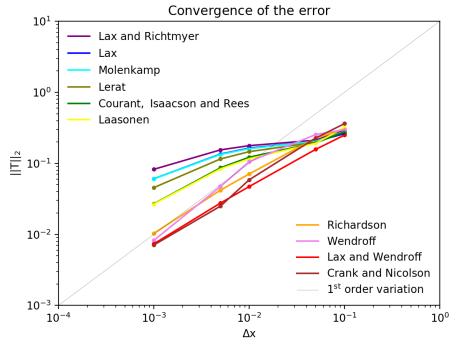

FIGURE 42. Convergence of the error plot for the traveling Gaussian wave, which we use to rank schemes. As found, the benefit of second order schemes is much more noticeable on a finer grid than on coarser grids.

Finally, although we have focused our study to understand and test both accuracy of each of the eleven low order finite difference schemes and the fact that they do not always reach desired convergence rate as well as their stabilities, the convergence studies carried out and showed in Fig. 42 (which agrees with Fig. 41) also lead to better ability to discriminate between schemes. Specifically, Fig. 42 compares the l^2-norm at different grid resolutions. As interestingly found and emphasized, the benefit of high order schemes is much more noticeable on a finer grid than on coarser grids. Besides we find performance achieved with the Lax-Wendroff scheme to be comparable to or better than performance with rest schemes in our sample, specifically the one with the decayless Crank-Nicholson scheme, the Lax-Wendroff scheme has the advantage of being more tractable numerically. In conclusion, the Lax-Wendroff oscillatory scheme of finite difference method provides the most successful description of advection equation of the A, and thus this result should be taken into consideration during the integration of the full heat-like equation subjected to some instabilities (future papers in the series will discuss on it); together with the corresponding result from Part I for the Schmidt's scheme.

4. **Concluding remarks**

The scope of this Part II is exactly to complete the analysis of Part I by studying the advective transport. To achieve this goal, we select and discuss a complete and unbiased sample of schemes for the advection parabolic partial differential equation constituted by all those up to second-order in both time and space; which are of topical current interest. We also put to precisely test such sample considering the Lagrange-Charpit problem in the presence of differentiable initial perturbations with discontinuous derivative; which appear in a wide variety of physical contexts. In other words, different schemes include both single-step and three-time-level, both explicit or hierarchical and non-explicit or monolithic, both consistent and inconsistent, both stable and unstable, both first-order accuracy and second-order accuracy, and both convergent and divergent; while each scheme includes discretizations which obviously are both reliable or robust and inaccurate or uncertain. In fact, we perform a complete study of each behavior and its implication on the error estimation of each scheme. Moreover, we empirically validate as well as illustrate all of this phenomenology by computation.

To be more precise, the classical Richardson's [6], Schmidt's [8], Crank-Nicolson [9], Laasonen's [11], Courant-Isaacson-Rees [12], Lax's [13], Lax-Richtmyer [14], Wendroff's [15], Lax-Wendroff [16], Molenkamp's [17] and Lerat's [18] schemes for a advection type transport equation have been coherently revised at low and (which is a vital aspect to capture the correct behavior of the system in the regions where the space scale is very small) high wavenumbers by exploiting the power of both the reverse Taylor's analysis [3] and the discrete Fourier's analysis [4], even though these associated formalisms are not physically equivalent. In fact, this distinction is important because we demonstrate these mode high wavenumbers (smallest scales) always remain poorly constrained. At the same time, the Courant-Friedrichs-Lewy condition have been reinterpreted as the instantaneous velocity sign flip with no damping in an explicit scheme. For more clarity, we homogeneously test all the schemes on an equal spatiotemporal discretization by performing an a priori minimization best-fit. In fact, we highlight the benefits of this framework. In addition, we use all of them to probe the Lax-Richtmyer theorem [14] and also the Godunov's theorem [5], which has in practice a significant effect on advective transport. Our main conclusions are summarized below.

(1) The pioneering Richardson's numerical scheme for approximating the solution to advection linear equation is a one step three time level scheme which naturally presents a unphysical computational mode propagating in opposite direction. The Richardson's solution presents no damping of Fourier modes but additionally shows moderate numerical dispersion which does however not resolve the high frequency Fourier harmonics. Nevertheless, the first benefit is not as desirable as it may seem, as it does not prevent his conditional instability. We also reveal spurious oscillations in the numerical solution. In particular, it is shown that the Richardson's numerical solution that use the constraint $C = 1$ reduces to the exact outcome of the linear type differential equation.
(2) The simplest Schmidt's numerical scheme for advection differential equation unfortunately presents a positive damping coefficient, and therefore is invalid for advective transport in general. We even provide numerical simulations of a test case based on this scheme.
(3) The innovative Crank-Nicolson numerical scheme for the advection equation is also dissipation free but additionally shows moderate numerical dispersion which does however not resolve the

high frequency Fourier harmonics. Nevertheless, we show that Crank-Nicolson solution exhibits only one acceleration regime with respect to C away from the exact solution, explaining its stability. Such benefit, generally speaking, can be only observed in non-explicit solutions of advection-like equations. We also reveal spurious oscillations in the numerical solution. This scheme, however, remains a good approximation when applies to an usual nonmonotone initial-value problem for the linear advection equation.

(4) The curious Laasonen's numerical scheme presents moderate damping and additionally shows moderate numerical dispersion which does however not resolve the high frequency Fourier harmonics. Nevertheless, we show that Laasonen's solution exhibits only one acceleration regime with respect to C explaining its stability; in stark contrast with his explicit counterpart, the Schmidt's scheme. We also reveal, on the other hand, no spurious oscillations in the numerical solution.

(5) The impressive Courant-Isaacson-Rees scheme presents a rapid uniform damping, which is able to explain their two acceleration with respect to C regimes until their conditional instability. Addditionally, we show that Courant-Isaacson-Rees solution exhibits only moderate numerical dispersion; however, it is both selective during its acceleration regimen and uniform in its deceleration regimen, i.e. which does not resolve the high frequency Fourier harmonics except for $C \geq 0.5$. We also reveal, on the other hand, no spurious oscillations in the numerical solution. In particular, it is finally shown that the Courant-Isaacson-Rees numerical solution that use $C = 1$ reduces to the exact outcome of the linear type differential equation; however, any other C value suffers a poor decoupling.

(6) The intriguing Lax's numerical scheme presents a quadratic consistency restriction which produces a very poor numerical dispersion; which is in fact both atypical and anomalous for the faster and higher frequency visible Fourier harmonics. Additionally, we also show that Lax's solution exhibits strong selective damping which does however not prevent his conditional instability. We also reveal spurious oscillations in the numerical solution. Finally, it is particularly shown that the Lax's numerical solution that use $C = 1$ reduces to the exact outcome of the linear type

differential equation; however, any other C value also suffers a poor decoupling.

(7) The peculiar Lax-Richtmyer numerical scheme presents strong selective damping and additionally shows moderate numerical dispersion which does however not resolve the high frequency Fourier harmonics. Nevertheless, we show that Lax-Richtmyer solution exhibits only one acceleration regime with respect to C explaining its stability; in dramatic contrast with his explicit counterpart, the Lax's scheme. We also reveal, on the other hand, no spurious oscillations in the numerical solution.

(8) The surprising Wendroff's numerical scheme does not create damping and presents only one acceleration regime with respect to C towards the exact solution. However, we demonstrated that this does not prevent his marginal stability because his (computationally diffusive) nonexplicit nature. Additionally, we also demonstrated that Wendroff's solution exhibits strong uniform dispersion which also implies very low accuracy in the faster and higher frequency visible Fourier waves. We also reveal spurious oscillations in the numerical solution. Finally, it is particularly shown that the Wendroff's numerical solution that use $C = 1$ also reduces to the exact outcome of the linear type differential equation.

(9) The ingenious Lax-Wendroff numerical scheme presents an uniform damping, which is able to explain their two acceleration regimes with respect to C: the one in lower but close to $C = \sqrt{0.5}$, and another until their conditional instability. We also show that Lax-Wendroff solution exhibits only moderate numerical dispersion; however, it is both selective for $C \leq \sqrt{0.5}$ and uniform for $C > \sqrt{0.5}$, i.e. which does not resolve the high frequency Fourier harmonics except for $C \geq \sqrt{0.5}$. We also reveal spurious oscillations in the numerical solution. Finally, it is particularly shown that the Lax's numerical solution that use $C = 1$ reduces to the exact outcome of the linear type differential equation. This scheme also is the preferred approximation when apply it to an usual nonmonotone initial-value problem for the linear advection equation.

(10) The strange Molenkamp's numerical scheme presents very strong uniform damping and additionally shows strong numerical dispersion which does not resolve the high frequency Fourier harmonics.

Nevertheless, we show that Molenkamp's solution exhibits only one acceleration regime with respect to C explaining its stability; in contrast with his explicit counterpart, the Courant-Isaacson-Rees scheme. We also reveal, on the other hand, no spurious oscillations in the numerical solution.

(11) The elaborated Lerat's numerical scheme presents strong uniform damping and additionally shows very strong numerical dispersion which does however not resolve the high frequency Fourier harmonics. Nevertheless, we show that Lerat's solution exhibits only one acceleration regime with respect to C explaining its stability; in sharp contrast with his explicit counterpart, the Lax-Wendroff scheme. We also reveal, on the other hand, no spurious oscillations in the numerical solution.

Despite its simplicity, this has however been a challenging project which contains numerous different scenarios. Indeed, the focus of the present paper was in rich variety of physical effects and numerical artifacts only little explored in the original literature, which are expressly relevant for high accuracy or data systematics. Overall, our findings, we believe, should help researchers entering the field, while contributing to the ongoing efforts to refine our understanding of the first order spatial derivative and its properties applicable in an accompanying paper where (mass or thermal) diffusion appears together with (heat and mass) advection. In fact, in third paper of the series we shall continue working the theory of difference schemes with both the physical help of the Fourier decomposition and the equivalent mathematical clarity of the theory of differential equations. Afterward we shall consider the non-linear case.

Statements and Declarations

Competing interests: The authors have no relevant financial or non-financial interests to disclose.

Data availability: No new data were created or analysed in this study.

Appendix A. The Lagrange-Charpit 1776 traveling Gaussian wave analytical solution as a test case

We begin with the one dimensional well posed (in the sense of Hadamard) problem given by the first order partial differential equation

$$\begin{cases} \frac{\partial T}{\partial t} = -v\,\frac{\partial T}{\partial x} & x \in (0,\, L),\, t > 0, \\ T(x,\, 0) = e^{-200\,(x-0.2)^2} & x \in (0,\, L). \end{cases} \tag{A.1}$$

in an enclosed spatial domain subject to some initial and boundary conditions. Specifically, we imagine that the heat energy from a smooth initial source flows or moves in a rod of length given only due to the flow determined by a constant velocity field. That is, we start with a Gaussian peak-shaped wave at the position $x = 0.2$ of the domain as a possible model for the heat source. We refer to this motion of thermal energy by the mechanism of moving mass in the rod as heat transfer.

Eq. (A.1) is the prototypical hyperbolic differential equation.

This test case guarantees the suitability of the formulation of the analytical solution.

Of course, this benchmark problem represents an idealized integrable situation but capture the main characteristics and numerical difficulties for hyperbolic equations. In Paper III we consider a number of additional issues, including a variable transport velocity, a source term, nonlinearities and higher dimensions.

Using the method of characteristics, we obtain the following solution to our initial value problem:

$$T(x,t) = e^{-200\,(x-0.2-v\,t)^2} \tag{A.2}$$

which merely translates the initial data at speed v as time progresses. We also obtain Eq. (A.2) using the standard method of separation of variables and Fourier transform.

Additionally, we represent this explicit solution in Figure 43 to graphically visualize how the initial profile translates to the right at constant speed without changing shape — which has to be simulated by the numerical solutions.

Acknowledgments

We thank Tapan K. Sengupta for his comments and insightful conversations.

References

[1] P. Sagaut, V. K. Suman, P. Sundaram, M. K. Rajpoot, Y. G. Bhumkar, S. Sengupta, A. Sengupta, T. K. Sengupta, Global spectral analysis: Review of numerical methods, *Computers and Fluids*, **261** (2023), 105915; doi:10.1016/j.compfluid.2023.105915

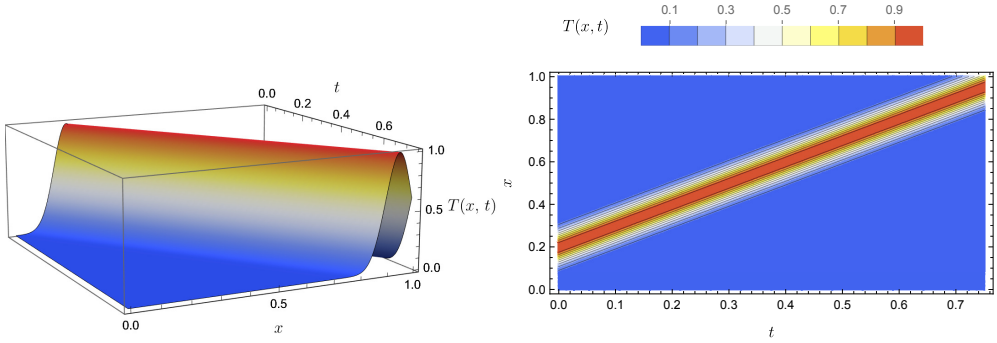

(A) 3-dimensional plot of $T(x,t)$ (B) Contour plot of $T(x,t)$

FIGURE 43. Representation of the analytical temperature distribution given by Eq. (A.2). The pseudo-colours indicate the temperature values. The contour lines are drawn at specific intervals of 0.1 units.

[2] G. Garrido, J. L. G. Pestaña, Revisiting finite difference solutions for heat-type equations. Part I. Diffusive transfer, *International Journal of Applied Mathematics*, **37(6)** (2024), 649-698; doi:10.12732/ijam.v37i6.6

[3] C. W. Hirt, Heuristic stability theory for finite-difference equations, *Journal of Computational Physics*, **2(4)** (1968), 339-355; doi:10.1016/0021-9991(68)90041-7

[4] J. von Neumann, R. D. Richtmyer, On the Numerical Solution of Partial Differential Equations of Parabolic Type, In: *Los Alamos Technical Reports*, LA–657 (1947).

[5] S. K. Godunov, Finite difference method for numerical computation of discontinuous solutions of the equations of fluid dynamics, *Matematičeskij Sbornik*, **47(89)** (1959), 271-306.

[6] L. F. Richardson, The approximate arithmetical solution by finite differences of physical problems involving differential equations, with an application to the stresses in a masonry dam, *Philosophical Transactions of the Royal Society of London, Series A*, **210** (1910), 307-357; doi:10.1098/rsta.1911.0009

[7] R. Courant, K. Friedrichs, H. Lewy, Über die partiellen Differenzengleichungen der mathematischen Physik, *Mathematische Annalen*, **100** (1928), 32-74; doi:10.1147/rd.112.0215

[8] E. Schmidt, Über die Anwendung der Differenzenrechnung auf technische Anheiz- und Abkühlungsprobleme, *Beiträge zur Technischen*

Mechanik und Technischen Physik: August Föppl zum Siebzigsten Geburtstag am 25. Januar 1924, (1924), 179-189; doi:10.1007/978-3-642-51983-3_19

[9] J. Crank, P. Nicolson, A practical method for numerical evaluation of solutions of partial differential equations of the heat-conduction type, *Mathematical Proceedings of the Cambridge Philosophical Society*, **43** (1947), 50-67; doi:10.1017/S0305004100023197

[10] L. H. Thomas, *Elliptic Problems in Linear Difference Equations over a Network*, Watson Sci. Comput. Lab. Rept., Columbia University (1949).

[11] P. Laasonen, Über eine Methode zur Lösung der Wärmeleitungs-gleichung, *Acta Mathematica*, **81** (1949), 309-317; doi:10.1007/BF02395025

[12] R. Courant, E. Isaacson, M. Rees, On the solution of nonlinear hyperbolic differential equations by finite differences, *Communications on Pure and Applied Mathematics*, **5** (1952), 243-255; doi:10.1002/cpa.3160050303

[13] P. D. Lax, Weak solutions of nonlinear hyperbolic equations and their numerical computation, *Communications on Pure and Applied Mathematics*, **7** (1954), 159-193; doi:10.1002/cpa.3160070112

[14] P. D. Lax, R. D. Richtmyer, Survey of the stability of linear finite difference equations, *Communications on Pure and Applied Mathematics*, **9** (1956), 267-293; doi:10.1002/cpa.3160090206

[15] B. Wendroff, Finite difference approximations to solutions of partial differential equations, *New York University ProQuest Dissertations Publishing* (1958), 6102619.

[16] P. D. Lax, B. Wendroff, Systems of conservation laws, *Communications on Pure and Applied Mathematics*, **13**, (1960), 217-237; doi:10.1002/cpa.3160130205

[17] C. R. Molenkamp, Accuracy of Finite-Difference Methods Applied to the Advection Equation, *Journal of Applied Meteorology*, **7(2)** (1967), 160-167; doi:10.1175/1520-0450(1968)007<0160:AOFDMA>2.0.CO;2

[18] A. Lerat, Une classe de schémas aux différences implicites pour les systèmes hyperboliques de lois de conservation, *Comptes Rendus Acad. Sc. Paris*, **Sér. A 288** (1979), 1033-1036.